3

Interaction of Light and Dielectric Media

Optical components and waveguiding fiber are designed to control the interaction between light and media. The regime of interest in this text is material transparency, to first order. Transparent glasses, crystals, and garnets are the building blocks on which passive optical components and optical fiber are made. Moreover, the interactions addressed in this text are optically linear in that the material response is assumed linear with field intensity. This is not actually the case since, for example, optical fiber has a prominent Kerr effect, but linearity will do for the studies to follow. An equally broad topic is the interaction between light and semiconductors such as diode lasers and optical detectors, but such interactions are not covered here.

The main purpose of this chapter is to introduce elementary classical descriptions for the constitutive relations of isotropic, anisotropic, gyrotropic, and optically active materials, and to detail how these constitutive relations, when included in Maxwell's equations, change the wavefront, power flow, and polarization of light. Glasses and birefringent crystals, principal examples of isotropic and anisotropic materials, are well characterized by classical wave-electron interaction. Faraday rotation induced by diamagnetic materials, a particular example of a gyrotropic material, yields to classical analysis, but a quantum-mechanical model is necessary to describe rotation in ferrimagnetic garnets. Finally, a constitutive relation of optical activity based on a classical description can be sketched to give flavor, but a detailed dipole-dipole interaction model is really necessary.

There are two levels of treatment for the interaction of light and media. First a constitutive relation must be found that dictates how the incident field effects the dipole moments (and possibly free electrons) of the material, and how these dipole moments in turn effect the field. Second, Maxwell's equations are solved based on the inclusion of the constitutive relation. The solution of Maxwell's equations, in this context, is completely classical and the rigorous treatment of the kDB system is provided.

Jay N. Damask: Polarization Optics in Telecommunications, SSOS 101, 79–142 (2005)

3.1 Introduction of Media Terms into Maxwell's Equations

The modifications to Maxwell's equations to include media terms are treated first. Overall, the equations must show how light behaves within a bulk, homogeneous medium and at the interface into and out of the region. In vacuum an electromagnetic wave is described by electric and magnetic fields **E** and **H**. Within a material, however, the wave is described by the electric and magnetic flux densities **D** and **B**. The flux densities incorporate the original field and the media reaction. The following sections then classify possible interaction types and recast Maxwell's equations for solution within a material.

When an electromagnetic wave propagates through a material, the electric and magnetic fields couple to bound and free electrons. A material with free electrons is conductive and any currents that are generated by the field absorb energy from that field and impart loss. A material without free electrons is dielectric. The travelling field forces the bound electrons to oscillate and they, in turn, radiate. In a pure dielectric without impurities, the induced radiation field is not diffuse but instead co- and counter-propagates with the incident field, so, when combined, the total field has a shortened wavelength and slowed energy flow.

There are two interactions to account for when light propagates within a dielectric medium: the radiation field from electronic dipoles that are stimulated by the incident field; and the radiation field from magnetic dipoles, or current loops, that are likewise stimulated. The electric field can directly couple to the electric dipoles and the magnetic field can directly couple to the magnetic dipoles. There can also be cross-coupling where the electric field induces magnetic dipole radiation and the magnetic field induces electric dipole radiation, as is the case in a chiral medium.

First the electric-dipole radiation. Including paired charge density ρ_p and unpaired (or free) charge density ρ_u, Gauss' law for the electric field is

$$\nabla \cdot \varepsilon_o \mathbf{E} = \rho_p + \rho_u \tag{3.1.1}$$

A dielectric, non-conductive medium has only paired charges since every electron is bound to an atom; the unpaired charge density is zero, $\rho_u = 0$. Without free electrons there is no current, so $\mathbf{J} = 0$ as well. For incident field energies below the ionization energy, the field stimulates the electrons to oscillate. To first order atomic nuclei do not move, so the electrons move closer and further away from the nucleus to generate a oscillating dipole. The oscillation frequency matches the frequency of the incident field.

The electric dipole moment of the oscillator is $\mathbf{p} = -\mathrm{e}\mathbf{r}$, where $-\mathrm{e}$ is the electron charge and $\mathbf{r}$ is the vector distance between electron and nucleus. Vector $\mathbf{r}$ points in the direction of positive charge. The polarization density vector $\mathbf{P}$ of the media is the product of the individual dipole moments and the number of dipoles N per unit volume, or

$$\mathbf{P} = -N\mathrm{e}\mathbf{r} \tag{3.1.2}$$

As the electrons oscillate, the electric charge changes position. A differential volume $\mathrm{d}V$ containing a charge density N has at any time a charge of $q = -\mathrm{e}\,\mathbf{r}\cdot\mathrm{d}\mathbf{a}$ exterior to its volume, where $\mathrm{d}\mathbf{a}$ is a differential surface-area element. The total net charge Q remaining on the interior comes from integrating across the surface,

$$Q = -\oint_S (N\mathrm{e}\mathbf{r})\cdot\mathrm{d}\mathbf{a}$$

Rewriting Q in terms of dipole density $\mathbf{P}$, Gauss' integral law shows that

$$\oint_S \mathbf{P}\cdot\mathrm{d}\mathbf{a} = \int_V \nabla\cdot\mathbf{P}\;\mathrm{d}V$$

The net charge within volume V is then

$$Q = -\int_V \nabla\cdot\mathbf{P}\;\mathrm{d}V$$

But by definition, the net charge Q within the same volume due to the paired charge density ρ_p is

$$Q = \int_V \rho_p\;\mathrm{d}V$$

Comparing these two expressions for charge density, the paired charge density is related to the divergence of the polarization density by

$$\rho_p = -\nabla\cdot\mathbf{P} \tag{3.1.3}$$

Substitution back into Gauss' law gives

$$\nabla\cdot(\varepsilon_o\mathbf{E} + \mathbf{P}) = 0 \tag{3.1.4}$$

So now it is clear how to define the electric-flux density $\mathbf{D}$:

$$\mathbf{D} = \varepsilon_o\mathbf{E} + \mathbf{P}, \quad \text{and} \quad \nabla\cdot\mathbf{D} = 0 \tag{3.1.5}$$

where $\mathbf{D}$ has units of $(\mathrm{C/m^2})$ and the electric-flux density has zero divergence.

Next comes magnetic-dipole radiation. Gauss' law for the magnetic field is

$$\nabla\cdot\mu_o\mathbf{H} = 0 \tag{3.1.6}$$

The divergence of the field is zero because there is no magnetic monopole. Magnetic fields and the currents that generate them must close on themselves. The elementary model for a unit magnet is a current loop having current i circulating along a perfect conductor having radius R enclosing area $\mathbf{a}$, where

the direction of $\mathbf{a}$ is normal to the surface element. The magnetic dipole moment $\mathbf{m}$ can be identified as $\mathbf{m} = i\mathbf{a}$. In analogy with the electric polarization density, the magnetization density $\mathbf{M}$ is defined as

$$\mathbf{M} = N\mathbf{m}$$

Now, in the far-field, the scalar potentials of an electric dipole and magnetic dipole have the same form, provided that the magnetic dipole is identified as $\rho_m = \mu_o m$ [8]. So, in analogy with (3.1.3), the magnetic density is defined as

$$\rho_m = -\nabla \cdot \mu_o \mathbf{M} \tag{3.1.7}$$

Introducing of ρ_m into Gauss' magnetic law gives

$$\nabla \cdot (\mu_o \mathbf{H} + \mu_o \mathbf{M}) = 0 \tag{3.1.8}$$

In parallel with the electric-flux density $\mathbf{D}$, the magnetic-flux density $\mathbf{B}$ is defined by

$$\mathbf{B} = \mu_o \mathbf{H} + \mu_o \mathbf{M}, \quad \text{and} \quad \nabla \cdot \mathbf{B} = 0 \tag{3.1.9}$$

where $\mathbf{B}$ has units of (V-s/m^2), or the derived unit of (Tesla).

All materials at the very least exhibit the magnetic effects of nuclear and electronic spin. In general the resultant magnetic fields close on themselves on an atomic scale and therefore average out on a macro-scale. Moreover, a magnetic moment has an angular moment and any reorientation of that moment has a delay with respect to a sinusoidal driving field. At optical frequencies the induced magnetization, e.g. of a ferrite, is essentially zero. Bianisotropic materials exhibit a helical molecular structure or crystalline structure which can combine to couple the electric and magnetic fields via dipole and current excitation. These materials cause optical activity and are of growing importance in telecommunications since liquid crystal structures have a helical component.

Having defined the electric and magnetic flux densities $\mathbf{D}$ and $\mathbf{B}$, they must be incorporated into Faraday's and Ampère's laws. Faraday's law says that the curl of $\mathbf{E}$ is generated by the time variation of a field $\mathbf{F}$:

$$\nabla \times \mathbf{E} = -\frac{\partial}{\partial t}\,\mathbf{F}$$

Taking the divergence of both sides yields

$$\nabla \cdot (\nabla \times \mathbf{E}) = -\frac{\partial}{\partial t} \nabla \cdot \mathbf{F} = 0$$

Since the divergence of a solenoidal field is zero, the divergence of $\mathbf{F}$ must be constant: $\nabla \cdot \mathbf{F} = c_m$. Since $\nabla \cdot \mathbf{D} = 0$, the flux density $\mathbf{D}$ is a suitable field to include in Faraday's law. The same analysis holds for Ampère's law. Therefore one can restate Maxwell's equations in terms of $\mathbf{D}$ and $\mathbf{B}$:

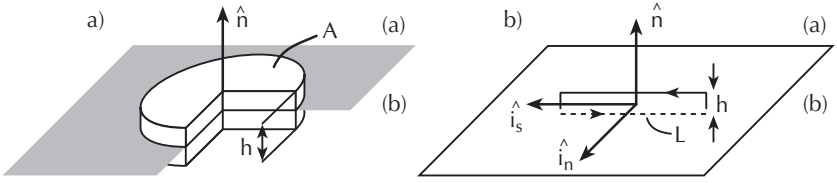

Fig. 3.1. Analysis of electric and magnetic flux density continuity across a boundary. a) Electric flux density continuity determined by a "pillbox" across the surface. b) Magnetic flux density continuity determined by a loop through the surface.

$$\nabla \times \mathbf{E} = -\frac{\partial}{\partial t}\mathbf{B} \tag{3.1.10a}$$

$$\nabla \times \mathbf{H} = \frac{\partial}{\partial t}\mathbf{D} \tag{3.1.10b}$$

The electric and magnetic flux densities are now fully incorporated into Maxwell's equations. In order to use these equations, constitutive relations that relate the polarization $\mathbf{P}$ and magnetization $\mu_o\mathbf{M}$ to the electric and magnetic fields are required. Constitutive relations determine these interactions.

Normal to an interface the electric and magnetic flux densities are continuous. Tangent to a surface the electric and magnetic fields are continuous. These continuity conditions are derived as follows.

The continuity condition for fluxes are derived from Gauss' law. Consider a small volume V in the shape of a pillbox that intersects a smooth, charge-free interface between two homogeneous regions denoted by (a) and (b) (Fig. 3.1(a)). The volume has height h and area normal to the interface A. Also, a unit vector $\hat{\mathbf{n}}$ points from region (b) to (a). Integration of $\nabla \cdot \mathbf{D} = 0$ over the volume and taking the limit to zero height gives

$$\begin{aligned}\lim_{h\to 0}\int_V \nabla\cdot\mathbf{D}\,\mathrm{d}V &= \lim_{h\to 0}\oint_S \mathbf{D}\cdot\mathrm{d}\mathbf{a}\\ &= \lim_{h\to 0}\left(\hat{\mathbf{n}}\cdot\left(\mathbf{D}^{(a)}-\mathbf{D}^{(b)}\right)A + h\int_C \mathbf{D}\cdot\mathrm{d}\mathbf{s}\right)\\ &= 0\end{aligned}$$

where S is the surface enclosed by volume V, C is the contour around area element A, and Stokes integral law is used to transform from volume to surface integrals. The electric flux density normal to the interface is therefore continuous:

$$\hat{\mathbf{n}}\cdot\left(\mathbf{D}^{(a)}-\mathbf{D}^{(b)}\right) = 0 \tag{3.1.11}$$

The normal component of the electric field, however, is not continuous. Just consider the step between vacuum and a dielectric:

$$\hat{\mathbf{n}}\cdot\left(\varepsilon_o\mathbf{E}^{(a)} - (\varepsilon_o\mathbf{E}^{(b)} + \mathbf{P}^{(b)})\right) = 0$$

Table 3.1. Inclusion of Electric and Magnetic Media Terms in Maxwell's Equations

$\nabla \cdot \varepsilon_o \mathbf{E} = -\nabla \cdot \mathbf{P}$	$\nabla \cdot \mu_o \mathbf{H} = -\nabla \cdot \mu_o \mathbf{M}$
$\mathbf{P} = -N\mathrm{e}\mathbf{r}$	$\mathbf{M} = N\mathbf{m}$
$\nabla \cdot (\varepsilon_o \mathbf{E} + \mathbf{P}) = 0$	$\nabla \cdot (\mu_o \mathbf{H} + \mu_o \mathbf{M}) = 0$
$\nabla \times \mathbf{H} = \dfrac{\partial}{\partial t} (\varepsilon_o \mathbf{E} + \mathbf{P})$	$\nabla \times \mathbf{E} = -\dfrac{\partial}{\partial t} (\mu_o \mathbf{H} + \mu_o \mathbf{M})$
$\mathbf{D} = \varepsilon_o \mathbf{E} + \mathbf{P}$	$\mathbf{B} = \mu_o \mathbf{H} + \mu_o \mathbf{M}$
$\mathbf{D}$: (C/m^2)	$\mathbf{B}$: (Vs/m^2)
$\hat{\mathbf{n}} \cdot \left(\mathbf{D}^{(b)} - \mathbf{D}^{(a)} \right) = 0$	$\hat{\mathbf{n}} \cdot \left(\mathbf{B}^{(b)} - \mathbf{B}^{(a)} \right) = 0$
$\hat{\mathbf{n}} \times \left(\mathbf{E}^{(b)} - \mathbf{E}^{(a)} \right) = 0$	$\hat{\mathbf{n}} \times \left(\mathbf{H}^{(b)} - \mathbf{H}^{(a)} \right) = 0$

The amplitude of $\mathbf{E}^{(b)}$ must take into account the strength of $\mathbf{P}^{(b)}$ for this relation to hold.

Using Gauss' law for the magnetic flux gives, via the same analysis

$$\hat{\mathbf{n}} \cdot \left(\mathbf{B}^{(a)} - \mathbf{B}^{(b)} \right) = 0 \tag{3.1.12}$$

The normal component of the magnetic flux density is continuous across an interface.

The tangential continuity conditions are derived from Faraday's and Ampère's laws. Consider a small loop that intersects the same interface (Fig. 3.1(b)). The area of the loop is A and its normal i_n is parallel to the interface. Integration of (3.1.10a) and taking the limit of zero height yields

$$\lim_{h \to 0} \int_S \nabla \times \mathbf{E} \cdot \mathrm{d}\mathbf{a} = -\lim_{h \to 0} \frac{\partial}{\partial t} \int_S \mathbf{B} \cdot \mathrm{d}\mathbf{a}$$

Separate evaluation of the integrals gives

$$\lim_{h \to 0} \oint_C \mathbf{E} \cdot \mathrm{d}\mathbf{s} = \lim_{h \to 0} \hat{\mathbf{i}}_s \cdot \left(\mathbf{E}^{(a)} - \mathbf{E}^{(b)} \right) L$$

and

$$-\lim_{h \to 0} \frac{\partial}{\partial t} \int_S \mathbf{B} \cdot \mathrm{d}\mathbf{a} = -\lim_{h \to 0} \frac{\partial}{\partial t} \hat{\mathbf{i}}_n \mathbf{B} h L$$

Using the identities $\hat{\mathbf{i}}_s = \hat{\mathbf{i}}_n \times \hat{\mathbf{n}}$ and $\mathbf{a} \cdot (\mathbf{b} \times \mathbf{c}) = (\mathbf{a} \times \mathbf{b}) \cdot \mathbf{c}$, the integrals produce the continuity law for the tangential electric field:

$$\hat{\mathbf{n}} \times \left(\mathbf{E}^{(a)} - \mathbf{E}^{(b)} \right) = 0 \tag{3.1.13}$$

The same analysis of Ampère's law gives the continuity condition for the tangential magnetic field:

$$\hat{\mathbf{n}} \times \left(\mathbf{H}^{(a)} - \mathbf{H}^{(b)} \right) = 0 \tag{3.1.14}$$

Table 3.1 summarizes the results of this section.

3.2 Constitutive Relation Tensors

The preceding section introduced polarization $\mathbf{P}$ and magnetization $\mu_o \mathbf{M}$ terms into Maxwell's equations. These terms are derived from the radiation fields of bound electrons within a dielectric medium. The radiation fields are themselves excited by incident electromagnetic waves; the combined incident and radiated fields inextricably co- and counter-propagate throughout the medium. The combined electric and magnetic fields are denoted by $\mathbf{D}$ and $\mathbf{B}$ and are called the electric and magnetic flux densities, respectively. Maxwell's equations including the flux densities are

$$\nabla \times \mathbf{E}(\mathbf{r}, t) = -\frac{\partial}{\partial t} \mathbf{B}(\mathbf{r}, t) \tag{3.2.1a}$$

$$\nabla \times \mathbf{H}(\mathbf{r}, t) = \frac{\partial}{\partial t} \mathbf{D}(\mathbf{r}, t) \tag{3.2.1b}$$

$$\nabla \cdot \mathbf{D}(\mathbf{r}, t) = 0 \tag{3.2.1c}$$

$$\nabla \cdot \mathbf{B}(\mathbf{r}, t) = 0 \tag{3.2.1d}$$

A specific medium is modelled by the relation between the field terms $\mathbf{E}$ and $\mathbf{H}$ and the flux density terms $\mathbf{D}$ and $\mathbf{B}$. The most general form of these constitutive relations is

$$\begin{pmatrix} c\mathbf{D} \\ \mathbf{H} \end{pmatrix} = \begin{pmatrix} \mathsf{P} & \mathsf{L} \\ \mathsf{M} & \mathsf{Q} \end{pmatrix} \begin{pmatrix} \mathbf{E} \\ c\mathbf{B} \end{pmatrix} \tag{3.2.2}$$

where c is the speed of light and P, L, M, and Q are 3×3 matrix tensors. The form of (3.2.2) is preferred for its invariance to relativistic transformation [11]. The constitutive tensors are generally frequency dependent, and when cast in time-harmonic form, are generally complex quantities.

Materials are classified according to the matrix entries of (3.2.2). When the cross-coupling terms L and M are non-zero, the medium is called bianisotropic. Optically active materials are bianisotropic. When the cross-coupling terms are zero ($\mathsf{L} = \mathsf{M} = 0$) then the medium is anisotropic. Within anisotropic materials the electric field excites only the electric flux, and the magnetic field excites only the magnetic flux. These excitations are generally not spatially uniform and depend on the eigenvectors of P and Q. Isotropy is a special

case of anisotropy in that P and Q are diagonal tensors with all entries equal. Physically, excitation of dipole moments is spatially uniform for isotropic materials.

The materials considered in this text are lossless to first order. Losslessness imposes certain symmetry conditions on the constitutive tensors. These conditions are determined by Poynting's conservation theorem. The Poynting's theorem derived from time-harmonic versions of (3.2.1a,b) is

$$\nabla \cdot (\mathbf{E} \times \mathbf{H}^*) = j\omega \, (\mathbf{E} \cdot \mathbf{D}^* - \mathbf{H}^* \cdot \mathbf{B})$$

Losslessness requires that the divergence of time-averaged power flow vanishes:

$$\langle \nabla \cdot \mathbf{S} \rangle = \frac{1}{2} \, \Re\mathrm{e} \Big[\, \mathrm{j}\omega \, (\mathbf{E} \cdot \mathbf{D}^* - \mathbf{H}^* \cdot \mathbf{B}) \Big] = 0 \tag{3.2.3}$$

To evaluate the impact of this constraint on the constitutive relations, expression (3.2.2) is re-ordered to put the fields on one side and the flux densities on the other:

$$\begin{pmatrix} \mathbf{D} \\ \mathbf{B} \end{pmatrix} = \mathbf{C}_{EH} \begin{pmatrix} \mathbf{E} \\ \mathbf{H} \end{pmatrix}, \quad \text{and} \quad \begin{pmatrix} \mathbf{E} \\ \mathbf{H} \end{pmatrix} = \mathbf{C}_{DB} \begin{pmatrix} \mathbf{D} \\ \mathbf{B} \end{pmatrix} \tag{3.2.4}$$

where

$$\mathbf{C}_{EH} = \begin{pmatrix} \varepsilon & \xi \\ \zeta & \mu \end{pmatrix}, \quad \text{and} \quad \mathbf{C}_{DB} = \begin{pmatrix} \kappa & \xi^i \\ \zeta^i & \nu \end{pmatrix} \tag{3.2.5}$$

The entries of $\mathbf{C}_{EH}$ and $\mathbf{C}_{DB}$ are, generally, 3×3 tensors.

Fluxes $\mathbf{D}$ and $\mathbf{B}$ in (3.2.3) can now be expressed in terms as $\mathbf{E}$ and $\mathbf{H}$. With the identity $\mathbf{E} \cdot \varepsilon^* \cdot \mathbf{E}^* = \mathbf{E}^* \cdot \varepsilon^\dagger \cdot \mathbf{E}$ and a similar one for $\mathbf{H}$ and μ, the lossless condition imposes the following constraints on the tensors of $\mathbf{C}_{EH}$ and $\mathbf{C}_{DB}$:

$$\varepsilon = \varepsilon^\dagger, \quad \mu = \mu^\dagger, \quad \xi = \zeta^\dagger \tag{3.2.6}$$

and

$$\kappa = \kappa^\dagger, \quad \nu = \nu^\dagger, \quad \xi^i = \zeta^{i\dagger} \tag{3.2.7}$$

Losslessness forces the on-diagonal tensors to be Hermitian and the off-diagonal tensors to posses symmetry. Accordingly, transmission through any such media retains a real-valued dispersion relation and is therefore lossless.

Tensors ξ and ζ are non-zero for bianisotropic media and identically zero for anisotropic media. Lossless isotropic materials have scalar (ε, μ), rather than tensor (ε, μ) values. In anisotropic and isotropic materials, ε and μ are readily identified as the electric permittivity and magnetic permeability tensors. Likewise, κ and ν are identified as the impermittivity and impermeability tensors, where

$$\kappa = \varepsilon^{-1}, \quad \text{and} \quad \nu = \mu^{-1} \tag{3.2.8}$$

For anisotropic and isotropic materials, the fields and flux densities are decoupled:

$$\mathbf{D} = \varepsilon \cdot \mathbf{E} \tag{3.2.9a}$$

$$\mathbf{B} = \mu \cdot \mathbf{H} \tag{3.2.9b}$$

Only when ε and μ are scalars are the fluxes necessarily aligned to the fields. Otherwise, fields and fluxes align along the eigenvectors of their respective tensors.

Finally, Poynting's theorem restated to include explicit time dependence is

$$\nabla \cdot \mathbf{S} + \frac{\partial W}{\partial t} = 0 \tag{3.2.10}$$

where the total stored energy is

$$W = \frac{1}{2} \left(\mathbf{E} \cdot \mathbf{D} + \mathbf{H} \cdot \mathbf{B} \right) \tag{3.2.11}$$

In the time-domain picture, losslessness requires an instantaneous response of the polarization and magnetization densities to the applied electro-magnetic field; a phase lag of $\mathbf{D}$ to $\mathbf{E}$, or $\mathbf{B}$ to $\mathbf{H}$, generates loss in the medium.

3.3 The *kDB* System

Section §3.1 showed that within a medium the incident fields and induced dipole radiation propagate together as electric and magnetic flux densities. These flux densities are the natural terms in which to describe the electromagnetic behavior. There is a second reason why these are the natural terms, and that is because the k-vector always lies perpendicular to plane-wave solutions of $\mathbf{D}$ and $\mathbf{B}$. One could instead consider using the fields $\mathbf{E}$ and $\mathbf{H}$ as descriptors within a medium since the Poynting vector always lies perpendicular to the fields: $\mathbf{S} = \mathbf{E} \times \mathbf{H}$. The choice of which system to use is made by looking for mathematical simplicity, not on physical grounds. Since the k-vector always lies perpendicular to $\mathbf{D}$ and $\mathbf{B}$, one of three vectors drops out of Maxwell's equations. Thus the so-called kDB system is introduced. Once the fluxes are everywhere determined, the fields are calculated from the inverse constitutive relations and, ultimately, the Poynting vector is determined.

The kDB system is constructed to take advantage of that natural basis defined by the triplet $(\mathbf{k}, \mathbf{D}, \mathbf{B})$. Plane-wave solutions separate the oscillatory term $\exp\{j(\omega t - \mathbf{k} \cdot \mathbf{r})\}$ from a slowly varying and (piecewise) spatially independent flux envelope. Maxwell's equations (3.2.1) are thus recast as

$$\mathbf{k} \times \mathbf{E} = \omega \mathbf{B} \tag{3.3.1a}$$

$$\mathbf{k} \times \mathbf{H} = -\omega \mathbf{D} \tag{3.3.1b}$$

$$\mathbf{k} \cdot \mathbf{D} = 0 \tag{3.3.1c}$$

$$\mathbf{k} \cdot \mathbf{B} = 0 \tag{3.3.1d}$$

The natural coordinates for these flux vectors and k-vector are $(\hat{e}_1, \hat{e}_2, \hat{e}_3)$. In particular, $\hat{e}_3$ always points along the k-vector ($\mathbf{k} = \hat{e}_3 k$) and the $\mathbf{D}$ and $\mathbf{B}$ vectors line in the DB plane defined by $(\hat{e}_1, \hat{e}_2)$ normal to $\hat{e}_3$ (Fig. 3.2). The result is that $D_3 = B_3 = 0$ when resolved on the kDB coordinate system. This provides the promised simplification.

Typically the constitutive tensors are written along their eigenvectors. The permittivity tensor for a birefringent crystal, for example, is generally written with only diagonal entries. However, the flux densities can propagate in an arbitrary direction. To reconcile the two reference frames, the eigenvector frame of the tensors, denoted by coordinate system (x, y, z), is rotated into the natural frame of the fluxes and k-vector. This transformation is done with the rotation operator T, which defines a first rotation about z and a second rotation about $\hat{e}_1$, the latter being the local x axis. Thus

$$\begin{aligned} T &= R_x(\theta) R_z(\phi) \\ &= \begin{pmatrix} 1 & 0 & 0 \\ 0 & \cos\theta & -\sin\theta \\ 0 & \sin\theta & \cos\theta \end{pmatrix} \begin{pmatrix} \cos\phi & -\sin\phi & 0 \\ \sin\phi & \cos\phi & 0 \\ 0 & 0 & 1 \end{pmatrix} \end{aligned}$$

For vectors A and A_k resolved in the crystal and flux coordinates, respectively, the forward and inverse vector transformations are

$$A_k = TA, \quad \text{and} \quad A = T^{-1} A_k$$

where

$$T = \begin{pmatrix} \cos\phi & -\sin\phi & 0 \\ \cos\theta\sin\phi & \cos\theta\cos\phi & -\sin\theta \\ \sin\theta\sin\phi & \sin\theta\cos\phi & \cos\theta \end{pmatrix} \tag{3.3.2}$$

and $T^{-1} = T^T$. The operators T and T^{-1} are unitary: $TT^{-1} = I$.

When acting on matrices rather than vectors, the transformation operator T imparts a similarity transform on the coordinate system, cf. §2.4.4. Given the kDB constitutive relation

$$\begin{pmatrix} \mathbf{E} \\ \mathbf{H} \end{pmatrix} = \begin{pmatrix} \boldsymbol{\kappa} & \boldsymbol{\xi}^i \\ \boldsymbol{\zeta}^i & \boldsymbol{\nu} \end{pmatrix} \begin{pmatrix} \mathbf{D} \\ \mathbf{B} \end{pmatrix} \tag{3.3.3}$$

resolved on an underlying (x, y, z) coordinate system, the constitutive relation is rotated into the flux frame according to

$$\begin{pmatrix} \mathbf{E}_k \\ \mathbf{H}_k \end{pmatrix} = \begin{pmatrix} T \cdot \boldsymbol{\kappa} \cdot T^{-1} & T \cdot \boldsymbol{\xi}^i \cdot T^{-1} \\ T \cdot \boldsymbol{\zeta}^i \cdot T^{-1} & T \cdot \boldsymbol{\nu} \cdot T^{-1} \end{pmatrix} \begin{pmatrix} \mathbf{D}_k \\ \mathbf{B}_k \end{pmatrix} \tag{3.3.4a}$$

$$= \begin{pmatrix} \boldsymbol{\kappa}_k & \boldsymbol{\xi}^i_k \\ \boldsymbol{\zeta}^i_k & \boldsymbol{\nu}_k \end{pmatrix} \begin{pmatrix} \mathbf{D}_k \\ \mathbf{B}_k \end{pmatrix} \tag{3.3.4b}$$

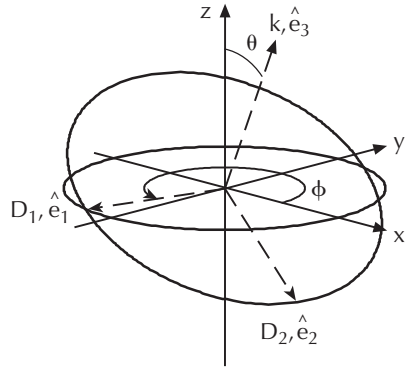

Fig. 3.2. The kDB coordinate system is written relative to a (x, y, z) coordinate system that is typically aligned to the eigenvectors of the constitutive tensors. First, a right-hand rotation about $\hat{z}$ by ϕ, then a right-hand rotation about the $\hat{e}_1$ axis by θ. Axis $\hat{e}_3$ is aligned to the k-vector, and $\hat{e}_1$ always lies in the (x, y) plane.

Each constitutive relation tensor is transformed by the coordinate-system change, but since T is unitary, there is no dilation or compression of the tensors, only a pure rotation.

Now, since $\mathbf{k} = k\,\hat{e}_3$ and $D_3 = B_3 = 0$, the fields $\mathbf{E}$ and $\mathbf{H}$ can be eliminated in (3.3.1a,b) to solve for $D_{1,2}$ and $B_{1,2}$. The resulting coupled equations are

$$\begin{pmatrix} \kappa_{11} & \kappa_{12} \\ \kappa_{21} & \kappa_{22} \end{pmatrix} \begin{pmatrix} D_1 \\ D_2 \end{pmatrix} = -\begin{pmatrix} \xi^i_{11} & \xi^i_{12} - u \\ \xi^i_{21} + u & \xi^i_{22} \end{pmatrix} \begin{pmatrix} B_1 \\ B_2 \end{pmatrix} \quad (3.3.5a)$$

$$\begin{pmatrix} \nu_{11} & \nu_{12} \\ \nu_{21} & \nu_{22} \end{pmatrix} \begin{pmatrix} B_1 \\ B_2 \end{pmatrix} = -\begin{pmatrix} \zeta^i_{11} & \zeta^i_{12} + u \\ \zeta^i_{21} - u & \zeta^i_{22} \end{pmatrix} \begin{pmatrix} D_1 \\ D_2 \end{pmatrix} \quad (3.3.5b)$$

where the phase velocity is defined as

$$u = \omega/k \quad (3.3.6)$$

As written, the tensor components κ_{ij}, ν_{ij}, ξ^i_{ij}, and ζ^i_{ij} are resolved in the kDB system. Depending on the complexity of the material, (3.3.5a,b) can be solved simultaneously, or either $\mathbf{D}_k$ or $\mathbf{B}_k$ can be eliminated and the resulting equation can be solved.

Equations (3.3.5a,b) are of the utmost importance to the description of electromagnetic propagation within dielectric media. These equations will be used in the following to determine the eigenmodes of propagation within a medium, the phase and group velocities, the dispersion relations, and the direction of energy flow. The elegance of the kDB system is that all linear, lossless materials can be described by this one system of equations, the particulars depending only on the tensor entries.

3.4 The Lorentz Force

As outlined in the introduction to the chapter, constitutive relations for isotropic, birefringent, gyrotropic, and optically active materials are derived from classical electron–wave interaction in the following. The Lorentz force and Newton's second law are sufficient to model simple behavior of isotropic and anisotropic media. Anisotropic media, of course, includes birefringent and gyrotropic materials. The constitutive relation for optical activity is derived heuristically as any robust model requires more work than space allows.

In isotropic and anisotropic materials the electric field couples to the bound electrons through the Lorentz force. The Lorentz force $\mathbf{f}$ is defined by

$$\mathbf{f} = -\mathrm{e}\left(\mathbf{E} + \frac{\partial \mathbf{r}}{\partial t} \times \mathbf{B}\right) \tag{3.4.1}$$

where $(-\mathrm{e})$ is the charge of the electron and $\mathbf{r}$ is the displacement of the electron from its neutral position. Since the electrons in lossless material are bound to the nucleus, the charge-attraction serves as a restoring force. For low-intensity light the electron displacement is purely linear, so one can take the restoring force K as constant with displacement $\mathbf{r}$. Newton's second law $\mathbf{f} = m\mathbf{a}$ generates the equation of motion for a bound electron driven by the Lorentz force:

$$m\frac{\partial^2 \mathbf{r}}{\partial t^2} = -K\mathbf{r} - \mathrm{e}\mathbf{E} - \mathrm{e}\frac{\partial \mathbf{r}}{\partial t} \times \mathbf{B} \tag{3.4.2}$$

In the absence of an externally applied magnetic field, the cross-product force $\mathbf{r}\times\mathbf{B}$ is vanishingly small compared to $\mathbf{E}$. Indeed, recast in time-harmonic form and substituting in Faraday's law gives $\mathbf{r} \times (\mathbf{k} \times \mathbf{E}) \rightarrow |r\omega/c|\,\mathbf{E}$. For $r \sim 0.1$Å and $\omega \sim 2\pi \times 200$ THz, $|rk| < 10^{-5}$. To turn the cross-product term "on" either an intense external magnetic field must be applied or the internal magnetization must be high, as is the case for materials with magnetic domains.

3.5 Isotropic Materials

The equation of motion for a bound electron in a linear isotropic material is

$$m\frac{\partial^2 \mathbf{r}}{\partial t^2} = -K\mathbf{r} - \mathrm{e}\mathbf{E} - m\gamma\frac{\partial \mathbf{r}}{\partial t} \tag{3.5.1}$$

where γ is a resonant damping coefficient, and the restorative and drag forces on the electron are centro-symmetric. The magnetic-induced force present in (3.4.2) is neglected. When an incident field is a plane wave at frequency ω, (3.5.1) is rewritten in time-harmonic form:

$$\left(-m\omega^2 + jm\gamma\omega + K\right)\mathbf{r} = -\mathrm{e}\mathbf{E} \tag{3.5.2}$$

The following subsection incorporates this equation of motion into Maxwell's equations to obtain a dispersion relationship and the functional forms for the material permittivity, refractive index, and absorption.

3.5.1 Permittivity of Isotropic Materials

Equation (3.1.2) relates the material polarization to the electron displacement. Multiplying (3.5.2) by $N\mathrm{e}$, the frequency dependence of the polarization density is

$$\mathbf{P} = \frac{N\mathrm{e}^2}{K - m\omega^2 + jm\gamma\omega}\,\mathbf{E} \tag{3.5.3}$$

The polarization $\mathbf{P}$ is a linear function of the applied electric field $\mathbf{E}$ and points in the same direction. The frequency-dependent coefficient is a resonant factor where the resonance frequency ω_o is defined as

$$\omega_o = \sqrt{K/m} \tag{3.5.4}$$

The resonance frequency is not a function of the field energy or intensity (to this order of approximation) and is therefore a fixed quantity that depends on the composition of the material.

The material susceptibility $\boldsymbol{\chi}_e$ is the tensor that relates $\mathbf{E}$ to $\mathbf{P}$ for linear media. For isotropic media the tensor is a scalar χ_e. The field and polarization are thus related via

$$\mathbf{P} = \varepsilon_o \chi_e(\omega)\mathbf{E} \tag{3.5.5}$$

Identifying (3.5.5) with (3.5.3), the complex susceptibility of a simple isotropic material is

$$\chi_e(\omega) = \frac{1}{m\varepsilon_o}\,\frac{N\mathrm{e}^2}{\omega_o^2 - \omega^2 + j\gamma\omega} \tag{3.5.6}$$

The susceptibility tensor or scaler is fundamental because it embodies the homogeneous response of a material.

Susceptibility χ_e is used to define permittivity in the following way. The electric-flux density $\mathbf{D}$ is the combination of the incident field and its induced dipole polarization:

$$\mathbf{D} = \varepsilon_o \mathbf{E} + \mathbf{P} = \varepsilon(\omega)\mathbf{E} \tag{3.5.7}$$

where (3.5.5) is used to define the material permittivity ε accordingly:

$$\varepsilon(\omega) = \varepsilon_o\,(1 + \chi_e(\omega)) \tag{3.5.8}$$

When the susceptibility is a tensor so is the permittivity. Often the permittivity relative to vacuum is used to compare materials. The relative permittivity ε_r is defined as

$$\varepsilon_r = \varepsilon/\varepsilon_o \tag{3.5.9}$$

By analogy to permittivity, material permeability μ is defined as $\mathbf{B} = \mu\mathbf{H}$. However, for materials considered here there is little or no interaction between the field and the magnetic moments of the material. Therefore, μ is treated as a scalar, frequency-independent quantity.

With the above definitions of the material permittivity and permeability, the Helmholtz wave equation is (compare (1.1.6) on page 3)

$$\nabla^2 \mathbf{E} = \mu\varepsilon \frac{\partial^2}{\partial t^2} \mathbf{E} \tag{3.5.10}$$

Plane-wave solutions of the form

$$\mathbf{E}(\mathbf{r}, t) = \mathbf{E}_o \exp\left(j\left(\omega t - \tilde{\mathbf{k}} \cdot \mathbf{r}\right)\right)$$

when inserted into (3.5.10), generate the dispersion relation

$$\tilde{k} = \omega\sqrt{\mu\varepsilon}$$

Now, the permittivity ε is a complex scalar, so $\tilde{k}$ is complex as well. That means absorption as well as retardation are fundamental implications of the Lorentz equation of electron motion.

The frequency dependence of the loss and refractive index of an isotropic material is found as follows. Expansion of the permittivity and dispersion relation into real and imaginary parts,

$$\varepsilon = \varepsilon' + j\varepsilon''$$

$$(k + j\alpha) = \frac{\omega}{c}\,(n + j\kappa)$$

gives an expression for the real and imaginary parts of the relative permittivity:

$$(n + j\kappa)^2 = \varepsilon_r' + j\varepsilon_r'' \,,$$

The real and imaginary parts of the relative permittivity are identified with the refractive index n and extinction coefficient κ as

$$\varepsilon_r' = n^2 - \kappa^2, \quad \text{and} \quad \varepsilon_r'' = 2n\kappa \tag{3.5.11}$$

Finally, expanding the resonant form of the susceptibility χ_e into its real and imaginary parts and identifying with (3.5.11) gives the coupled equations for the refractive index and extinction coefficient as

$$n^2 - \kappa^2 = 1 + \frac{N\mathrm{e}^2}{m\varepsilon_o} \frac{\omega_o^2 - \omega^2}{(\omega_o^2 - \omega^2)^2 + (\gamma\omega)^2} \tag{3.5.12}$$

and

$$2n\kappa = -\frac{N\mathrm{e}^2}{m\varepsilon_o} \frac{\gamma\omega}{(\omega_o^2 - \omega^2)^2 + (\gamma\omega)^2} \tag{3.5.13}$$

In the transparent regime, the bound-electron resonance is far away from the frequency of the incident field. In this case, $\kappa \simeq 0$ and the dispersion relation is approximately

$$k = \frac{\omega}{c}\, n \tag{3.5.14}$$

The phase velocity of the plane wave as it propagates within the medium is $v_{\mathrm{ph}} = c/n$. Inspection of (3.5.12) in light of $\kappa \simeq 0$ shows that the refractive

index n is greater than unity. This is generally the case, although exceptions are possible, such as in the x-ray region where multiple material resonances are below, rather than above, the excitation frequency. For the near-infrared transparent regime important to telecommunications, the refractive index is greater than one. Another implication of polarization of the material is the wavelength change within the medium. The wavelength in the material λ is related to the free-space wavelength λ_o as

$$\lambda = \lambda_o / n \tag{3.5.15}$$

That the wavelength is reduced is not surprising since the frequency of the light does not change whether the light is in vacuum or material, and $\lambda\omega = 2\pi v_{\text{ph}}$ always holds.

The phase velocity v_{ph} is the velocity of a monochromatic wavefront. However, the velocity of energy flow of a narrowband pulse is related to the frequency derivative of the wavenumber:

$$\frac{1}{v_{\text{g}}} = \frac{dk}{d\omega} \tag{3.5.16}$$

where v_{g} is the group velocity. As has been shown, even a simple dielectric material has permittivity dispersion, so the phase and group velocities generally differ. The group index n_g, defined by $v_{\text{g}} = c/n_g$, is

$$n_g = n - \lambda \frac{dn}{d\lambda} \tag{3.5.17}$$

Generally, material and waveguide dispersion has a negative index slope with wavelength. So, generally, the group index lies above the refractive index.

Now, the key simplification so far has been that a single resonance exists within the isotropic material. In general this is not the case. Multiple resonances can be related to various absorption bands of the atoms or molecules that constitute the material. A more robust model includes multiple resonances and weighs the contributions to the susceptibility according to the fraction of atoms that are associated with each resonance. Well into the transparent regime where the damping factor can be ignored, the refractive index square is modelled as

$$n^2(\omega) = 1 + \frac{N\text{e}^2}{m\varepsilon_o} \sum_n \frac{f_n}{\omega_o^2 - \omega^2}$$

Often an additional pole at low frequency and another at high frequency are added based on phenomenological experience. The refractive index equation is then

$$n^2(\omega) = 1 + \frac{a_\infty}{\omega_o^2} + \frac{N\text{e}^2}{m\varepsilon_o} \sum_n \frac{f_n}{\omega_o^2 - \omega^2} - \frac{a_o}{\omega^2}$$

Table 3.2. Atomic Lines for Abbe Number Definition

Wavelength (nm)	Symbol	Spectral line	Element
656.2725	C	Red hydrogen line	H
589.2938	d	Yellow sodium line	Na
587.5618	d	Yellow helium line	He
486.1327	F	Blue hydrogen line	H

Converting frequency ω to wavelength λ and introducing material-specific fitting coefficients, the Sellmeier equation for refractive index dispersion is

$$n^2(\lambda) = A + \sum_n \frac{B_n \lambda^2}{\lambda^2 - C_n} - D\lambda^2 \tag{3.5.18}$$

There are, in fact, any number of forms of this equation. While the measured refractive index data is absolute, the value of the coefficients in (3.5.18) depends on which equation is used to model the data. As an example of another form of the Sellmeier equation, the equation published by Schott Glass is

$$n^2(\lambda) - 1 = \frac{B_1 \lambda^2}{\lambda^2 - C_1} + \frac{B_2 \lambda^2}{\lambda^2 - C_2} + \frac{B_3 \lambda^2}{\lambda^2 - C_3} \tag{3.5.19}$$

The Abbe number is a measure of the refractive index dispersion throughout the visible region. The Abbe number generally works well for glasses rather than semiconductor or crystals because the amorphous, homogeneous nature of glass precludes strong resonances. The Abbe number v_d is defined on the d-line as

$$v_d = \frac{n_d - 1}{n_F - n_C} \tag{3.5.20}$$

where n_d, n_F, and n_C are the measured refractive indices on the d, F, and C lines, respectively. The wavelengths for these lines are defined in Table 3.2.

3.5.2 Propagation in Isotropic Materials

Even though the kDB system is intended for more complex propagation calculations, propagation within an isotropic material will be cast in this formalism for the sake of example. Within a material, one needs to find the directions of the k-vector and the Poynting vector, as well as the wavenumber. Also, the refraction properties into and out of the material needs to be determined; that is the topic of the following section.

In an isotropic material, tensors $\boldsymbol{\xi}^i$ and $\boldsymbol{\xi}^i$ in $\mathbf{C}_{DB}$ are zero, and κ and ν are scalars. The constitutive relations are

$$\begin{aligned} \mathbf{E} &= \kappa \mathbf{D} \\ \mathbf{H} &= \nu \mathbf{B} \end{aligned} \tag{3.5.21}$$

The underlying coordinate system is arbitrary. A rotation of the coordinate system into kDB coordinates leaves the constitutive relations unchanged since $T \cdot \kappa T^{-1} = \kappa$. Thus, substitution of (3.5.21) into the coupled kDB equations (3.3.5) gives

$$\kappa \begin{pmatrix} D_1 \\ D_2 \end{pmatrix} = \begin{pmatrix} 0 & u \\ -u & 0 \end{pmatrix} \begin{pmatrix} B_1 \\ B_2 \end{pmatrix} \tag{3.5.22a}$$

$$\nu \begin{pmatrix} B_1 \\ B_2 \end{pmatrix} = \begin{pmatrix} 0 & -u \\ u & 0 \end{pmatrix} \begin{pmatrix} D_1 \\ D_2 \end{pmatrix} \tag{3.5.22b}$$

Elimination of $\mathbf{B}$ generates the governing equation

$$\begin{pmatrix} u^2 - \nu\kappa & 0 \\ 0 & u^2 - \nu\kappa \end{pmatrix} \begin{pmatrix} D_1 \\ D_2 \end{pmatrix} = 0 \tag{3.5.23}$$

The electric field may be polarized along the $\hat{e}_1$ direction, the $\hat{e}_2$ direction, or a mixture of the two. For example, when the field is polarized along $\hat{e}_1$ then $D_1 \neq 0$ and $D_2 = 0$. In any case, the governing equation is satisfied when the phase velocity is

$$u = \sqrt{\nu\kappa} = \frac{1}{\sqrt{\mu\varepsilon}} \tag{3.5.24}$$

Substituting $u = \omega/k$ gives the dispersion relationship

$$k = \omega\sqrt{\mu\varepsilon} \tag{3.5.25}$$

from which the refractive index can be extracted:

$$n = \sqrt{\mu_r \varepsilon_r} \tag{3.5.26}$$

It is important to note that $|\mathbf{k}| = k$ and $k = \omega n/c$. Geometrically, the k-vector within the material can point in any direction, while the vector length is always k. The surface defined by all possible pointing directions of the k-vector is a sphere of radius $\omega n/c$:

$$k = \sqrt{k_x^2 + k_y^2 + k_z^2} \tag{3.5.27}$$

Finally, the Poynting vector is determined by the fields. Since κ and ν are scalars, the fields and respective flux densities are aligned. Since by definition the k-vector is aligned to $\hat{e}_3$, the Poynting vector is

$$\begin{aligned} \mathbf{S} &= \mathbf{E}_k \times \mathbf{H}_k \\ &= \nu\kappa\, \mathbf{D}_k \times \mathbf{B}_k \\ &= \frac{1}{\mu\varepsilon}\, \hat{e}_3 \end{aligned} \tag{3.5.28}$$

So, $\mathbf{k} \parallel \mathbf{S}$ in an isotropic material.

3.5.3 Refraction at an Interface

There are two questions to be addressed when dealing with refraction at a smooth interface: the angle of refraction, and the transmission and reflection coefficients. The refraction angle at an interface of two dissimilar isotropic materials is determined by the relative refractive indices alone and is independent of the polarization of the incident wave. The transmission and reflection coefficients, however, do depend on the incident polarization.

Phase matching of two waves, one in a first material and the other in a second material, is the single condition that must be satisfied along an interface. Refraction results when the refractive indices of the two materials differ. The canonical example is illustrated in Fig. 3.3(a). Here the plane wave k-vector in material 1 is inclined from the interface normal by θ_1. The wavelength within the material is $\lambda_1 = \lambda_o/n_1$ and the wave period as projected onto the interface is $\lambda_1/\sin\theta_1$. The same analysis applies to the second material, with θ_2 and n_2 in replacement. Phase matching at the interface requires

$$\frac{\lambda_1}{\sin\theta_1} = \frac{\lambda_2}{\sin\theta_2} \tag{3.5.29}$$

Snell's law is a restatement of (3.5.29) using the refractive index instead:

$$n_1 \sin\theta_1 = n_2 \sin\theta_2 \tag{3.5.30}$$

Since the refractive index of either (isotropic) material is independent of the polarization of the wave, the refraction angle is independent of polarization.

A geometric construction of refraction and reflection is illustrated in Fig. 3.3(b). Recall that within an isotropic medium the k-surface is a sphere having radius $\omega n/c$. The interface between two media bisects each sphere, dividing them into hemispheres of different radii. In Fig. 3.3(b) the refractive index of the first material is less than the second. The top and bottom half-circles represent the k-surfaces as projected onto the page, and the $\mathbf{k}_i$, $\mathbf{k}_t$, and $\mathbf{k}_r$ vectors are illustrated, subscripts i, t, and r referring to incident, transmitted, and reflected waves, respectively. Phase matching at the interface requires that the projection lengths of all three k-vectors match on the interface. In order for the tip of $\mathbf{k}_t$ to reach the $\omega n_2/c$ circle, the direction of $\mathbf{k}_t$ must change with respect to $\mathbf{k}_i$. For the reflected wave, however, $|\mathbf{k}_i| = |\mathbf{k}_r|$ and therefore the angle of the reflected wave is the same, albeit mirror-imaged about the normal to the interface. Finally, since these are isotropic materials, the Poynting and k-vectors for all three waves are aligned and coincident.

3.5.4 Reflection and Transmission for TE Waves

Next the reflection and transmission coefficients are determined. These coefficients are different for waves with transverse-electric (TE) and transverse-magnetic (TM) polarizations. The TE and TM polarization states are distinguished because, in the first case, the electric field oscillates in the plane of

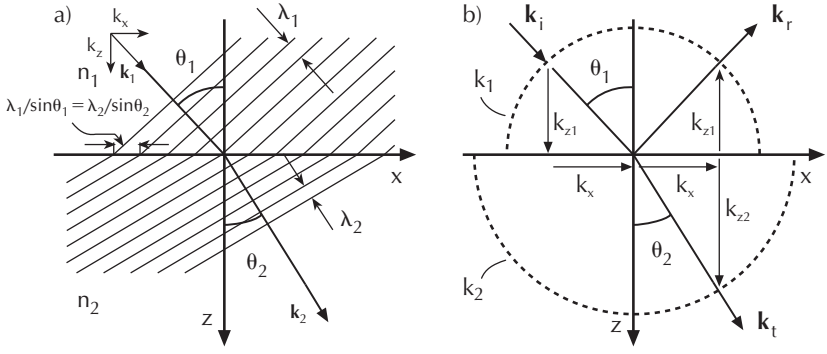

Fig. 3.3. Phase matching at a smooth dielectric interface. a) The free-space wavelength is reduced by the refractive index for waves within the dielectric. For $n_2 > n_1$ the wavelength in material 2 is shorter than that in material 1. Phase matching at the interface requires that the k-vector change direction at the interface. b) A k-vector diagram for refraction. The half-circle radii represent the respective refractive indices; the contours are circular in isotropic media. Phase matching requires the k_x vectors of both waves to match.

the interface while, in the second case, the magnetic field oscillates in that plane plane. The tangential continuity conditions (3.1.13-3.1.14) determine the relative field amplitudes in the two materials.

For TE plane waves, illustrated in Fig. 3.4(a), the total electric fields in the two materials are

$$\begin{aligned} \mathbf{E}_y^{(1)} &= \hat{y}E_o\left(\mathrm{e}^{-jk_{z1}z} + \Gamma\mathrm{e}^{jk_{z1}z}\right)\ \mathrm{e}^{-jk_x x} \\ \mathbf{E}_y^{(2)} &= \hat{y}E_o T\ \mathrm{e}^{-jk_{z2}z}\ \mathrm{e}^{-jk_x x} \end{aligned} \tag{3.5.31}$$

where Γ and T are complex coefficients of the reflection and transmission amplitudes, respectively. Faraday's law determines the associated magnetic fields:

$$\mathbf{H} = \frac{1}{j\omega\mu_o}\left(\hat{x}\frac{\partial}{\partial z}E_y - \hat{z}\frac{\partial}{\partial x}E_y\right)$$

where $\mathbf{E}_y = \hat{y}E_y$. The magnetic field components are therefore

$$\mathbf{H}_x^{(1)} = -\hat{x}\frac{k_{z1}}{\omega\mu_o}E_o\left(\mathrm{e}^{-jk_{z1}z} - \Gamma\mathrm{e}^{jk_{z1}z}\right)\ \mathrm{e}^{-jk_x x}$$

$$\mathbf{H}_x^{(2)} = -\hat{x}\frac{k_{z2}}{\omega\mu_o}E_y^{(2)}$$

and

$$\mathbf{H}_z^{(1,2)} = \hat{z}\frac{k_x}{\omega\mu_o}E_y^{(1,2)}$$

Only the tangential $\mathbf{E}$ and $\mathbf{H}$ field components are required to satisfy continuity across the interface. Application of the boundary conditions

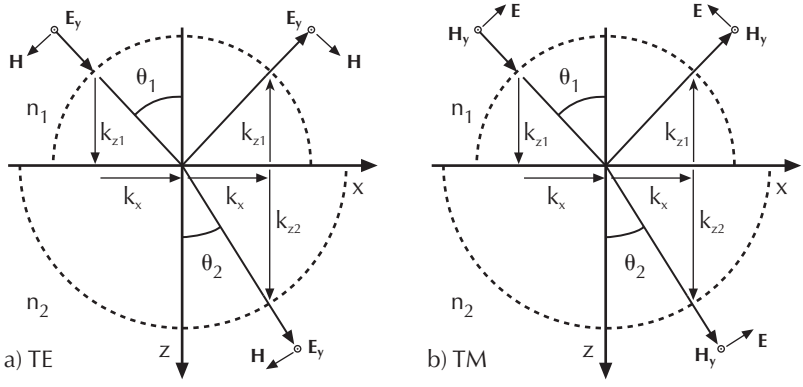

Fig. 3.4. Refraction diagrams for TE and TM waves. a) TE wave: the electric field lies tangential to the interface. b) TM wave: the magnetic field lies tangential to the interface.

$$\mathbf{E}_y^{(1)} = \mathbf{E}_y^{(2)} \quad \text{and} \quad \mathbf{H}_x^{(1)} = \mathbf{H}_x^{(2)}$$

on the interface where $x = 0$ gives

$$1 + \Gamma = T \tag{3.5.32a}$$

$$k_{z1}\,(1 - \Gamma) = k_{z2} T \tag{3.5.32b}$$

Combining (3.5.32a,b) gives the TE reflection coefficient in terms of material indices and ray angles:

$$\Gamma_{\text{TE}} = \frac{n_1 \cos\theta_1 - n_2 \cos\theta_2}{n_1 \cos\theta_1 + n_2 \cos\theta_2} \tag{3.5.33}$$

or, in terms of n_1 and θ_1 alone,

$$\Gamma_{\text{TE}} = \frac{\sqrt{1 - \sin^2\theta_1} - (n_2/n_1)\sqrt{1 - (n_1/n_2)^2 \sin^2\theta_1}}{\sqrt{1 - \sin^2\theta_1} + (n_2/n_1)\sqrt{1 - (n_1/n_2)^2 \sin^2\theta_1}} \tag{3.5.34}$$

Now, if one considers a box drawn around the point of incidence, then all the power that flows into the box from the incident wave must flow out of the box via the reflected and transmitted waves. The time-averaged Poynting vectors are

$$\langle S_i \rangle = \frac{1}{2\omega\mu_o}\ (\hat{x} k_x + \hat{z} k_{z1})\,|E_o|^2$$

$$\langle S_r \rangle = \frac{1}{2\omega\mu_o}\ (\hat{x} k_x - \hat{z} k_{z1})\,|\Gamma|^2 |E_o|^2$$

$$\langle S_t \rangle = \frac{1}{2\omega\mu_o}\ (\hat{x} k_x + \hat{z} k_{z2})\,|T|^2 |E_o|^2$$

Power conservation requires that

$$|\langle S_i \rangle| = |\langle S_r \rangle| + |\langle S_t \rangle| \tag{3.5.35}$$

Substitution of the TE Poynting vectors gives

$$1 = |\Gamma|^2 + \frac{n_2}{n_1}|T|^2$$

Defining $\mathrm{R} = |\Gamma|^2$ and $\mathrm{T} = n_2/n_1|T|^2$ generates the power conservation equation:

$$\mathrm{R} + \mathrm{T} = 1 \tag{3.5.36}$$

Clearly all that is reflected and transmitted must come from the incident power.

3.5.5 Reflection and Transmission for TM Waves

For TM plane waves, illustrated in Fig. 3.4(b), the magnetic field oscillates in the plane of the interface. In analogy to the TE wave solution, the total magnetic fields in the two materials are

$$\begin{aligned} \mathbf{H}_y^{(1)} &= \hat{y} H_o \left(\mathrm{e}^{-jk_{z1}z} + \Gamma \mathrm{e}^{jk_{z1}z} \right) \mathrm{e}^{-jk_x x} \\ \mathbf{H}_y^{(2)} &= \hat{y} H_o T \, \mathrm{e}^{-jk_{z2}z} \, \mathrm{e}^{-jk_x x} \end{aligned} \tag{3.5.37}$$

where Γ and T are complex coefficients of the TM-wave reflection and transmission amplitudes, respectively. The associated electric fields are determined from Ampère's law,

$$\mathbf{E} = -\frac{1}{j\omega\varepsilon}\left(\hat{x}\frac{\partial}{\partial z}H_y - \hat{z}\frac{\partial}{\partial x}H_y \right)$$

where $\mathbf{H}_y = \hat{y} H_y$. Solving for the fields and matching the tangential continuity condition across the interface yields

$$1 + \Gamma = T \tag{3.5.38a}$$

$$\frac{k_{z1}}{\varepsilon_1}(1 - \Gamma) = \frac{k_{z2}}{\varepsilon_2} T \tag{3.5.38b}$$

Combining (3.5.38a,b) gives the TM reflection coefficient in terms of material indices and ray angles:

$$\Gamma_{\mathrm{TM}} = \frac{n_2 \cos\theta_1 - n_1 \cos\theta_2}{n_2 \cos\theta_1 + n_1 \cos\theta_2} \tag{3.5.39}$$

or, in terms of n_1 and θ_1,

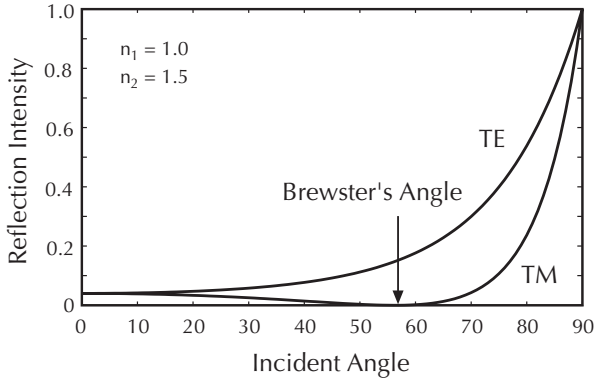

Fig. 3.5. Reflection intensities for TE and TM waves as a function of incident angle.

$$\Gamma_{\rm TM} = -\frac{\sqrt{1-\sin^2\theta_1} - (n_1/n_2)\sqrt{1-(n_1/n_2)^2\sin^2\theta_1}}{\sqrt{1-\sin^2\theta_1} + (n_1/n_2)\sqrt{1-(n_1/n_2)^2\sin^2\theta_1}} \tag{3.5.40}$$

Figure 3.5 compares the reflection intensities $|\Gamma|^2$ for TE and TM waves and an air-glass boundary as a function of incident angle. The TE reflection intensity increases monotonically, while the TM wave goes through a zero point along the way. The angle at which TM reflection is zero is called Brewster's angle.

The remarkable property of TM waves is that at Brewster's angle all reflection is extinguished. Brewster's angle satisfies the condition

$$\theta_1 + \theta_2 = \pi/2 \tag{3.5.41}$$

That is, the transmitted and reflected waves are perpendicular to one another (see Fig. 3.6(a)). That there is no power in the reflected wave is reasonable based on physical considerations. The radiation pattern of an electric dipole is null along the polar axis. Brewster's condition orients the dipole excitation and the direction of the reflected wave perpendicular to one another. Substituting Brewster's condition (3.5.41) into (3.5.39) gives the requisite incident angle θ_B

$$\theta_B = \tan^{-1}(n_2/n_1) \tag{3.5.42}$$

Brewster's condition cannot be satisfied by TE waves because the electric field of the reflected and transmitted waves are always parallel.

To write the power conservation equation in the form of (3.5.36), the reflection and transmission coefficients are identified to be

$$R = |\Gamma|^2, \quad \text{and} \quad T = \frac{n_1}{n_2}\,|T|^2$$

As a concluding remark, in addition to incident angle and polarization state, only the refractive-index ratio n_2/n_1 determines the refraction angle, not the absolute refractive indices.

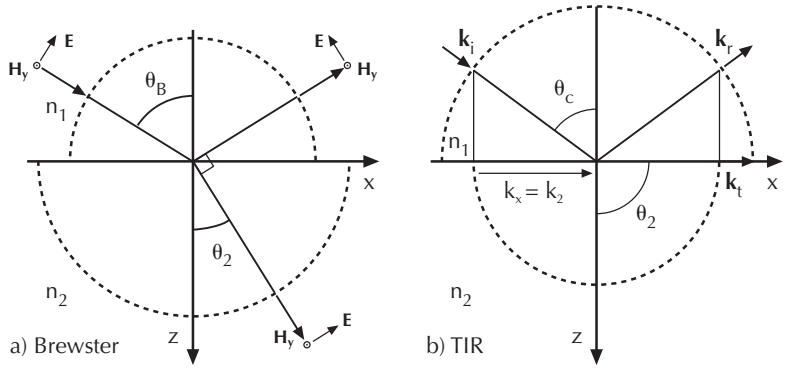

Fig. 3.6. a) The condition at Brewster's angle: the reflected and transmitted waves are perpendicular to one another. Brewster's condition of zero reflectance applies onto to TM waves. b) The critical angle for total internal reflection, $n_2 < n_1$.

3.5.6 Total Internal Reflection

Total internal reflection (TIR) occurs when the phase-matching condition at an interface cannot be satisfied by plane-wave solutions. A plane-wave solution does not exist when phase-matching requires a phase velocity that exceeds the speed of light. In this case all the incident power is reflected.

For TIR to exist, the refractive index in which the incident wave travels must exceed the refractive index beyond the interface: $n_1 > n_2$. This condition is required whether the material is isotropic or anisotropic. In isotropic media the refractive index is independent of polarization state, so TIR between two isotropic media is polarization agnostic.

For TIR to occur at an interface where $n_1 > n_2$, the incident angle must be at or beyond the critical angle. The critical angle for the incident wave is that angle which makes the transmitted wave run parallel to the interface $\theta_2 = \pi/2$ (see Fig. 3.6(b)). At and beyond the critical angle the wavefront period as projected onto the interface from the incident side is shorter than the wavelength of a plane wave on the transmission side. There is no orientation of $\mathbf{k}_t$ that achieves phase matching. Instead, k_t becomes imaginary and the transmitted field decays exponentially into the lower-index media.

Referring to Fig. 3.3(a), the angle where $\lambda_1 = \lambda_2 / \sin\theta_2$ is called the critical angle. Snell's law generates the relation

$$\theta_c = \sin^{-1} n_2/n_1 \tag{3.5.43}$$

Resolving k_2 into normal and transverse components,

$$k_2 = \sqrt{k_x^2 + k_{z2}^2}\ ,$$

at and above the critical angle $k_x > k_2$. This condition is only satisfied when k_z is imaginary:

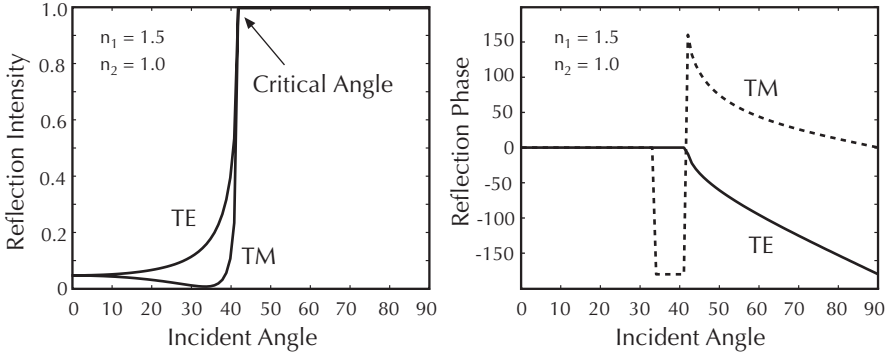

Fig. 3.7. Reflection intensity and phase before and after the onset of total internal reflection. a) Reflection intensity for TE and TM waves. b) Reflection phase shifts for TE and TM. Notice the sign change for TM reflection across the Brewster's angle boundary.

$$k_{z2} = j\alpha_{z2} = j\sqrt{k_x^2 - k_2^2}$$

This shows the exponential decay of the field along the axis normal to the surface. Parallel to the surface the incident and evanescent fields are phase matched.

In comparison to the reflected intensities from air to glass $n : 1.0 \to 1.5$ plotted in Fig. 3.5, the reflection intensity and phase for the reverse direction $n : 1.5 \to 1.0$ is plotted in Fig. 3.7. Since both media are isotropic the critical angle is the same for both polarizations. Below the critical angle of $\theta_c \simeq 41.8°$ the reflection coefficients are below unity and there is no phase slip. At and beyond the critical angle, however, the reflection coefficients are unity and a phase develops between the incident and reflected waves. The phase of the TM wave goes through a π phase shift at Brewster's angle.

When the incident angle exceeds the critical angle, the reflection coefficient takes unity magnitude and develops a phase shift. The phase shift is called the Goos-Hänchen shift. Defining the reflection phase as $\angle\Gamma = 2\phi$, the boundary conditions for TE (3.5.32) and TM (3.5.38) are rewritten as

$$1 + \mathrm{e}^{2j\phi} = T \tag{3.5.44a}$$

$$q_1(1 - \mathrm{e}^{2j\phi}) = q_2 T \tag{3.5.44b}$$

where for TE $q = k_z$ and for TM $q = k_z/\varepsilon$. The Goos-Hänchen phase shifts are

$$\phi_{\mathrm{TE}} = -\tan^{-1}\left(\frac{\alpha_{z2}}{k_{z1}}\right) \quad \text{and} \quad \phi_{\mathrm{TM}} = -\tan^{-1}\left(\frac{\varepsilon_1\alpha_{z2}}{\varepsilon_2 k_{z1}}\right) \tag{3.5.45}$$

Expanding in terms of the indices and incident angle, the reflection phases are

$$\angle\Gamma_{\mathrm{TE}} = -2\tan^{-1}\left[\frac{\sqrt{\sin^2\theta_1 - (n_2/n_1)^2}}{\cos\theta_1}\right] \tag{3.5.46a}$$

$$\angle\Gamma_{\mathrm{TM}} = -2\tan^{-1}\left[\frac{\sqrt{\sin^2\theta_1 - (n_2/n_1)^2}}{(n_2/n_1)^2\cos\theta_1}\right] \tag{3.5.46b}$$

The retardance $\Delta\Gamma$ induced by a TIR reflection, $\Delta\Gamma = (\angle\Gamma_{\mathrm{TE}} - \angle\Gamma_{\mathrm{TM}})$, is

$$\Delta\Gamma = 2\tan^{-1}\left(\frac{\cos\theta_1\sqrt{\sin^2\theta - (n_2/n_1)^2}}{\sin^2\theta_1}\right) \tag{3.5.47}$$

Since the sign of $\Delta\Gamma$ is positive, the magnitude of phase shift imparted on the TM wave is greater than that for the TE wave.

Total internal reflection can be understood as a partial penetration of the electro-magnetic wave into the material of lower index (cf. Fig. 3.8). The field component normal to the interface is a standing wave where the first null lies within the lower-index material. The phase shift between the interface location and the first field maxima is called the Goos-Hänchen shift. This shift is polarization dependent, as determined above, with the TM wave penetration greater than the TE penetration for the same inclination. Since the Goos-Hänchen phases differ for TE and TM waves, the state of polarization of a reflected field can be transformed with respect to the incident field.

For TE waves, the electric field expressions above the critical angle are

$$\mathbf{E}_y^{(1)} = \hat{y}2E_o\mathrm{e}^{j\phi}\cos(k_z z + \phi)\ \mathrm{e}^{-jk_x x} \tag{3.5.48a}$$

$$\mathbf{E}_y^{(2)} = \hat{y}E_o\mathrm{e}^{-j\alpha_z z}\mathrm{e}^{-jk_x x} \tag{3.5.48b}$$

The phase factor ϕ in the cosine term of the standing wave indicates that the last null of the standing wave lies below the interface and in region 2, Fig. 3.8(a). If the lower dielectric material were removed and a perfect metal conductor were placed at the location of the last null, the same standing wave pattern would persist.

The existence of the Goos-Hänchen phase shift alters the reflection diagrams of Fig. 3.4: the reflected light ray is no longer coincident with the incident ray at the interface. Rather, the incident ray penetrates into the lower material and reemerges forward-shifted with respect to its point of entry (Fig. 3.8(b)). The forward shift $2x_s$ is also rather confusingly called the Goos-Hänchen shift.

To construct the expression for the forward shift, consider two plane waves incident on the interface at slightly different angles $\theta_i \pm \Delta\theta$. The incident and reflected waves at $z = 0$ are

$$E_{y\pm}^{(i)} = E_o\ \mathrm{e}^{-j(k_x \pm \Delta k_x)x}$$

$$E_{y\pm}^{(r)} = E_o\ \mathrm{e}^{-j(k_x \pm \Delta k_x)x}\mathrm{e}^{2j(\phi\pm\Delta\phi)}$$

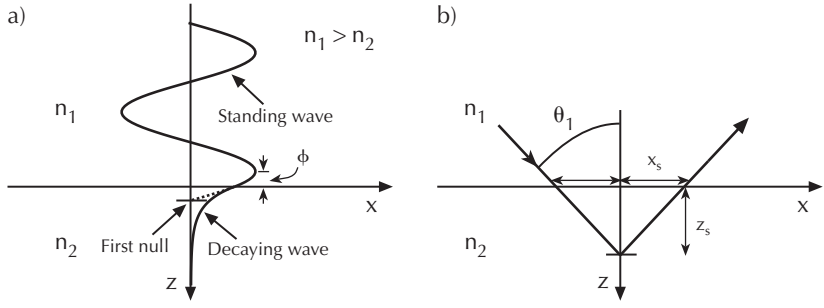

Fig. 3.8. Views of the Goos-Hänchen shift. a) A standing wave oscillates along the normal to the interface; the first null penetrates into the lower-index material. b) The inclined wave penetrates into the lower-index material and reemerges forward-shifted with respect to the incident wave. The penetration depth depends on the polarization state.

The total incident and reflected fields, summed over the two slightly different incident angles, are

$$E_y^{(i)} = 2E_o \cos(\Delta k_x x)\, \mathrm{e}^{-jk_x x} \tag{3.5.49a}$$

$$E_y^{(r)} = 2E_o \cos(\Delta k_x x - 2\Delta\phi)\, \mathrm{e}^{-jk_x x} \tag{3.5.49b}$$

Clearly the reflected field is shifted forward with respect to the incident field. Expanding the Goos-Hänchen shift about k_x gives

$$\phi(k + \Delta k_x) = \phi(k) + \frac{\partial \phi}{\partial k_x} \Delta k_x$$

Substitution into (3.5.49)(b) gives the expression for the reflected wave

$$E_y^{(r)} = 2E_o \cos(\Delta k_x (x - 2x_s))\, \mathrm{e}^{-jk_x x} \tag{3.5.50}$$

where the lateral Goos-Hänchen shift x_s is defined as

$$x_s = \frac{\partial \phi}{\partial k_x} \tag{3.5.51}$$

The Goos-Hänchen shifts for TE and TM reflections are therefore

$$x_s^{(\mathrm{TE})} = \frac{\tan\theta_1}{\sqrt{k_x^2 - k_2^2}} \tag{3.5.52a}$$

$$x_s^{(\mathrm{TM})} = \frac{x_s^{(\mathrm{TE})}}{\left(\dfrac{k_x}{k_2}\right)^2 + \left(\dfrac{k_x}{k_1}\right)^2 - 1} \tag{3.5.52b}$$

The penetration depth for TE incident light is

$$z_s = \frac{1}{\alpha_{z2}} \tag{3.5.53}$$

and the TM penetration is greater. The penetration depth of (3.5.53) makes sense since a point and slope fit to decaying field in (3.5.48b) gives the null location at α_{z2}^{-1}.

3.6 Birefringent Materials

Most glasses when unstrained are isotropic due to their amorphous nature and lack of long-range periodicity. Crystals, however, can exhibit anisotropy due do natural symmetries of the lattice structure. There are seven distinct crystalline classes, one class being cubic, where the atomic lengths of the three unit cell dimensions are equal; three classes having one unique and two identical unit cell dimensions; and three classes having different unit cell dimensions in all three directions. Cubic crystals, being centrosymmetric, are the only isotropic crystalline class. As the polarizability of a material is intimately related to the binding energy of electrons within the lattice, differences in unit cell dimensions of the remaining six classes cause differences in the material susceptibility. Accordingly, the dielectric constant of the material depends on how the bound electrons oscillate.

In the transparent regime, a high binding energy corresponds to a tight spring constant in the electron-oscillator model, which in turn corresponds to a high resonance frequency. A low binding energy corresponds to a low resonance frequency. At an excitation frequency ω below either resonance frequencies, the electron oscillation along the axis (axes) having lower resonance frequency will induce a higher refractive index (Fig. 3.9). A uniaxial crystal has two different refractive indices and a biaxial crystal has three different refractive indices. Both uniaxial and biaxial materials all called birefringent materials. Table 3.3 summarizes the correspondence of crystal class symmetries with susceptibilities.

When a linearly polarized light ray propagates through a crystal such that its electric field is aligned to a crystalline lattice axis, denoted by index i, the equation of motion for the bound electrons is

$$m\frac{\partial^2 r_i}{\partial t^2} = -K_i r_i - \mathrm{e}E_i - m\gamma_i \frac{\partial r_i}{\partial t} \tag{3.6.1}$$

where K_i and γ_i are the spring and damping constants for the i^{th} direction. In general, however, the electric fields are not aligned to a crystalline axis and multiple vibrational modes are excited. Substitution of electric susceptibility tensor $\boldsymbol{\chi}_e$ for the scalar χ_e provides the mathematical framework to describe this more complex oscillation. The tensor relation between the induced polarization density and incident electric field is

$$\mathbf{P} = \varepsilon_o \boldsymbol{\chi}_e(\omega)\mathbf{E} \tag{3.6.2}$$

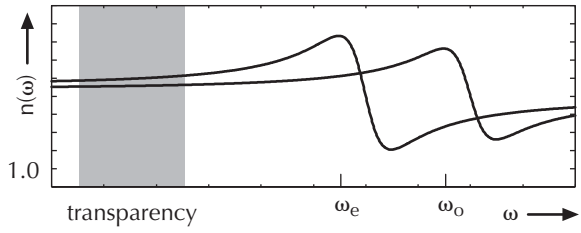

Fig. 3.9. Resonance model of birefringent vibrations and corresponding refractive index.

(cf. (3.5.5)). In the natural coordinate system of the crystal, the tensor $\boldsymbol{\chi}_e$ is written as

$$\mathbf{P} = \varepsilon_o \begin{pmatrix} \chi_a & & \\ & \chi_b & \\ & & \chi_c \end{pmatrix} \mathbf{E} \tag{3.6.3}$$

where each diagonal susceptibility may be different and all off-diagonal components are zero. The lack of off-diagonal components in the lattice coordinate system indicates that under pure excitation along a crystalline axis there is no coupling to the other axes.

That the susceptibility is a tensor recasts the dielectric constant ε as a tensor: $\boldsymbol{\varepsilon} = \varepsilon_o(1 + \boldsymbol{\chi}_e)$. The relation of $\mathbf{D}$ to $\mathbf{E}$, while still linear, now dependents on the orientation of the electric field. For example, in the kDB system, the electric constitutive relation is

$$\mathbf{D}_k = T \cdot \boldsymbol{\varepsilon} \cdot T^{-1} \mathbf{E}_k \tag{3.6.4}$$

The tensor $T \cdot \boldsymbol{\varepsilon} \cdot T^{-1}$ in general has off-diagonal components, mixing the electron oscillation modes. The following studies analyze the propagation and polarization states of light rays within birefringent media.

3.6.1 Propagation in Uniaxial Materials

Uniaxial birefringence exists in trigonal, tetragonal, and hexagonal crystals. The axis that has the unique lattice constant is called the extraordinary axis; the remaining two axes are call the ordinary axes. A uniaxial crystal can be positive uniaxial or negative uniaxial, depending of the relative refractive indices. The convention is

$$\begin{aligned} &\text{positive } (+) \text{ uniaxial} && n_e > n_o \\ &\text{negative } (-) \text{ uniaxial} && n_e < n_o \end{aligned}$$

Whether a crystal is positive or negative uniaxial depends on the particular constituents and group symmetries.

Table 3.3. Crystal Classes and Birefringence

Class	Unit cell	Susceptibility
Isotropic		
Cubic	$a = c = b$	$\boldsymbol{\chi}_e = \begin{pmatrix} \chi_a & & \\ & \chi_a & \\ & & \chi_a \end{pmatrix}$
Uniaxial		
Trigonal Tetragonal Hexagonal	$a = b \neq c$	$\boldsymbol{\chi}_e = \begin{pmatrix} \chi_o & & \\ & \chi_o & \\ & & \chi_e \end{pmatrix}$
Biaxial		
Triclinic Monoclinic Orthorhombic	$a \neq b \neq c$	$\boldsymbol{\chi}_e = \begin{pmatrix} \chi_a & & \\ & \chi_b & \\ & & \chi_c \end{pmatrix}$

After Fowles [5].

In an uniaxial material, tensors $\boldsymbol{\xi}^i$ and $\boldsymbol{\zeta}^i$ in C_{DB} are zero, $\boldsymbol{\nu}$ is a scalar, and $\boldsymbol{\kappa}$ is a tensor. The constitutive relations are

$$\mathbf{E} = \boldsymbol{\kappa} \cdot \mathbf{D} \tag{3.6.5a}$$

$$\mathbf{H} = \nu\, \mathbf{B} \tag{3.6.5b}$$

The impermittivity tensor $\boldsymbol{\kappa}$ is diagonal when $\mathbf{D}$ and $\mathbf{E}$ are aligned to its eigenvectors:

$$\kappa = \begin{pmatrix} \kappa_o & & \\ & \kappa_o & \\ & & \kappa_e \end{pmatrix} \tag{3.6.6}$$

where the subscripts o and e refer to ordinary and extraordinary axes, respectively. In diagonal form, $\kappa_i = 1/\varepsilon_i$. Moreover, the extraordinary axis is aligned to the $\hat{z}$ axis of the lattice.

A plane wave propagating within the crystal has a k-vector direction. In the kDB system the k-vector is always aligned to the $\hat{e}_3$ axis, while vectors D_1 and D_2 are aligned to $\hat{e}_1$ and $\hat{e}_2$, respectively. The fields and fluxes, after rotation into kDB coordinates from lattice coordinates, are governed by the coordinate-transformed constitutive relations

$$\mathbf{E}_k = \boldsymbol{\kappa}_k \cdot \mathbf{D}_k \tag{3.6.7a}$$

$$\mathbf{H}_k = \nu \mathbf{B}_k \tag{3.6.7b}$$

where $\boldsymbol{\kappa}_k = T \cdot \boldsymbol{\kappa} \cdot T^{-1}$, or

$$\boldsymbol{\kappa}_k = \begin{pmatrix} \kappa_o & & \\ & \kappa_o \cos^2\theta + \kappa_e \sin^2\theta & (\kappa_o - \kappa_e)\sin\theta\cos\theta \\ & (\kappa_o - \kappa_e)\sin\theta\cos\theta & \kappa_o \sin^2\theta + \kappa_e \cos^2\theta \end{pmatrix} \tag{3.6.8}$$

The impermittivity tensor $\boldsymbol{\kappa}_k$ is independent of ϕ: a uniaxial crystal is isotropic in the plane normal to $\hat{z}$, so the orientation of the k-vector-projection within that plane makes no difference. Substitution of (3.6.7) into the coupled kDB equations (3.3.5) gives

$$\begin{pmatrix} \kappa_{11} & \\ & \kappa_{22} \end{pmatrix} \begin{pmatrix} D_1 \\ D_2 \end{pmatrix} = \begin{pmatrix} 0 & u \\ -u & 0 \end{pmatrix} \begin{pmatrix} B_1 \\ B_2 \end{pmatrix}$$

$$\nu \begin{pmatrix} B_1 \\ B_2 \end{pmatrix} = \begin{pmatrix} 0 & -u \\ u & 0 \end{pmatrix} \begin{pmatrix} D_1 \\ D_2 \end{pmatrix}$$

where

$$\kappa_{11} = \kappa_o$$

$$\kappa_{22} = \kappa_o \cos^2\theta + \kappa_e \sin^2\theta$$

Elimination of $\mathbf{B}$ generates the governing equation

$$\begin{pmatrix} u^2 - \nu\kappa_{11} & 0 \\ 0 & u^2 - \nu\kappa_{22} \end{pmatrix} \begin{pmatrix} D_1 \\ D_2 \end{pmatrix} = 0 \tag{3.6.9}$$

In general, there are three non-trivial solutions to (3.6.9). They are

(1) $D_1 \neq 0, D_2 = 0 \qquad u = \pm\sqrt{\nu\kappa_{11}}$

(2) $D_1 = 0, D_2 \neq 0 \qquad u = \pm\sqrt{\nu\kappa_{22}}$

(3) $D_1 \neq 0, D_2 \neq 0 \qquad u = \pm\sqrt{\nu\kappa_{11}}$ and $u = \pm\sqrt{\nu\kappa_{22}}$

For solutions (1) and (2) the k-vector can point in any direction. The dispersion relation for solution (1) is

$$k = \frac{\omega}{c}\, n_o \tag{3.6.10}$$

Physically, the D_1 flux vector lies along $\hat{e}_1$, which in turn always lies in the (x, y) lattice plane. The D_1 vector therefore never excites the extraordinary vibrational mode; only the ordinary refractive index is experienced. One the other hand, the dispersion relation for solution (2) is

$$k = \frac{\omega}{c}\left[\frac{\cos^2\theta}{n_o^2} + \frac{\sin^2\theta}{n_e^2}\right]^{-1/2} \tag{3.6.11}$$

Physically, the D_2 flux vector can point in any direction in the lattice coordinates. Whether D_2 excites the extraordinary vibrational mode, the ordinary

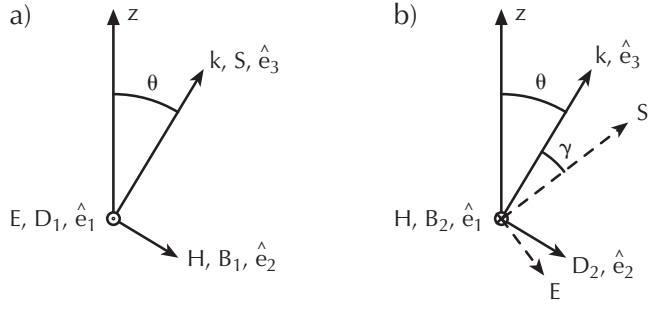

Fig. 3.10. Two solutions to linearly polarized propagation in a (−) uniaxial medium. a) $\mathbf{D} \perp \hat{z}$, therefore $\mathbf{S} \parallel \mathbf{k}$. b) $\mathbf{D} \not\perp \hat{z}$, therefore $\mathbf{S} \nparallel \mathbf{k}$. For a (+) uniaxial crystal, $\mathbf{S}_e$ lies between $\hat{z}$ and $\mathbf{k}$.

vibrational mode, or a mixture, depends only on θ, the declination angle of the k-vector to the $\hat{z}$ axis. The effective index n_{eff} is defined by identifying terms in (3.6.10, 3.6.11):

$$n_{\text{eff}} = \frac{n_e n_o}{\sqrt{n_e^2 \cos^2\theta + n_o^2 \sin^2\theta}} \tag{3.6.12}$$

When the k-vector is aligned with $\hat{z}$, $n_{\text{eff}} = n_o$; and when the k-vector is perpendicular to $\hat{z}$, $n_{\text{eff}} = n_e$. Otherwise, a mixture of vibrational modes is excited and an intermediate refractive index is experienced.

The characteristic direction of the Poynting vectors is another fundamental difference between solutions (1) and (2). As illustrated in Fig 3.10, the k- and Poynting vectors are aligned for solution (1) and are misaligned for solution (2). For solution (1), $D_2 = 0$ and the Poynting vector is

$$\begin{aligned} \mathbf{D}_k &= \hat{e}_1 D_1, \quad \mathbf{E}_k = \hat{e}_1 \kappa_{11} D_1 \\ \mathbf{B}_k &= \hat{e}_2 u/v D_1, \quad \mathbf{H}_k = \hat{e}_2 u D_1 \\ \mathbf{S}_k &= \hat{e}_3 \kappa_{11} u D_1{}^* D_1 \end{aligned} \tag{3.6.13}$$

In this case $\mathbf{S}_k \parallel \mathbf{k}$. Figure 3.10(a) illustrates that the D_1 vector is perpendicular to $\hat{z}$ and that k- and Poynting vectors are aligned. Solution (2) on the other hand, where $D_1 = 0$, generates a Poynting vector according to

$$\begin{aligned} \mathbf{D}_k &= \hat{e}_2 D_2, \quad \mathbf{E}_k = \hat{e}_2 \kappa_{22} D_2 + \hat{e}_3 \kappa_{32} D_2 \\ \mathbf{B}_k &= -\hat{e}_1 u/v D_2, \quad \mathbf{H}_k = -\hat{e}_1 u D_2 \\ \mathbf{S}_k &= (\hat{e}_3 \kappa_{22} - \hat{e}_2 \kappa_{32})\, u D_2{}^* D_2 \end{aligned} \tag{3.6.14}$$

This is a characteristically different solution. The **E** field has a longitudinal component along **k** and the Poynting vector is no longer parallel to the k-vector, $\mathbf{S}_k \nparallel \mathbf{k}$. Planes of constant phase lie perpendicular to the k-vector by definition, but those planes are tilted with respect to the energy-flow propagation direction. The walkoff angle γ between the ordinary and extraordinary Poynting vectors is

$$\begin{aligned} \tan\gamma &= -\frac{\kappa_{32}}{\kappa_{22}} \\ &= -\frac{(n_e^2 - n_o^2)\sin\theta\cos\theta}{n_e^2\cos^2\theta + n_o^2\sin^2\theta} \end{aligned} \tag{3.6.15}$$

The angle γ is a signed value: $\mathbf{S}_e$ is inclined further from the $\hat{z}$ axis than **k** in a positive uniaxial material; $\mathbf{S}_e$ is inclined less than **k** from $\hat{z}$ in a negative uniaxial material. In either case, $\mathbf{S}_e$ lies in the $(\hat{z}, \hat{k})$ plane. Similar to the reflection and transmission coefficients at a boundary, γ is a function of the n_e/n_o ratio.

There is an important rule for behavior of uniaxial crystals. The rule is

$\mathbf{D} \parallel \hat{z}$ or $\mathbf{D} \perp \hat{z} \Longrightarrow \mathbf{S}_e \parallel \mathbf{k}_e$	When the electric flux vector is either parallel or perpendicular to the $\hat{z}$ axis of the crystal, the extraordinary k- and Poynting vectors coincide.
$\mathbf{D} \nparallel \hat{z}$ or $\mathbf{D} \not\perp \hat{z} \Longrightarrow \mathbf{S}_e \nparallel \mathbf{k}_e$	When the electric flux vector is aligned in any other orientation, the extraordinary k- and Poynting vectors are misaligned.

Many designs use the fact that the ordinary and extraordinary rays can be separated by walkoff in a uniaxial crystal.

Returning to (3.6.9), solution (3) allows for the simultaneous existence of D_1 and D_2, but only when **k** is aligned along $\hat{z}$. With $D_1 \neq 0$ and $D_2 \neq 0$, (3.6.9) can only be satisfied for $\theta = 0$. Physically, the k-vector points along $\hat{z}$ and the perpendicular plane contains only the ordinary vibrational mode; only the ordinary refractive index is experienced and the material appears isotropic.

In general, only linearly polarized plane waves can propagate in a uniaxial birefringent crystal. There are two solutions for each orientation of the k-vector, each solution having a distinct wavenumber, effective refractive index, and polarization. An arbitrarily polarized light ray incident on a birefringent crystal is decomposed into two linearly polarized light rays, one associated with each wavenumber. Refraction into and out of a birefringent crystal shows the distinction between these two solutions.

The behavior of light in a birefringent medium, and its refraction into and out of the medium, is described geometrically by the indicatrix. The

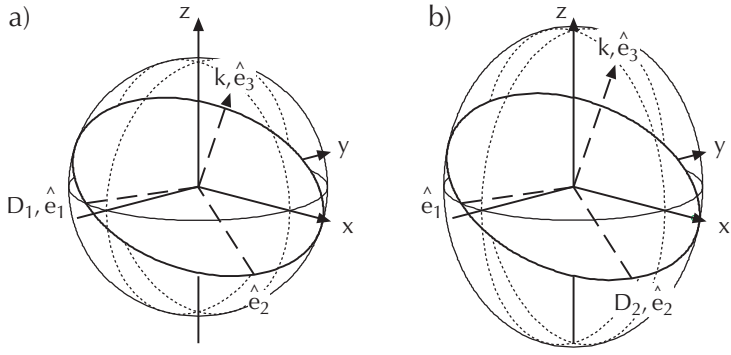

Fig. 3.11. The ordinary and extraordinary indicatrices. a) The ordinary indicatrix is isotropic to k-vector orientation. b) The extraordinary indicatrix is an ellipsoid, with major axis along $\hat{z}$. This is a negative uniaxial indicatrix, the $\hat{z}$ axis being longer than the others.

indicatrix encompasses all possible effective refractive indices of the medium, is associated with the k-vector and polarization vectors, and generates the orientation of the Poynting vector.

For each k-vector there are two indicatrices: one for $D_1 \neq 0$ and the other for $D_2 \neq 0$. In the former case, dispersion relation (3.6.10) is isotropic. Resolving the k-vector into components along the lattice coordinates, the ordinary indicatrix is a sphere (Fig. 3.11(a)), which follows the expression

$$\frac{k_x^2}{n_o^2} + \frac{k_y^2}{n_o^2} + \frac{k_z^2}{n_o^2} = \frac{\omega^2}{c^2} \tag{3.6.16}$$

For the $D_2 \neq 0$ case, the following coordinate associations are made:

$$\begin{aligned} k_z &= k\cos\theta \\ k_y &= k\sin\theta\sin\phi \\ k_x &= k\sin\theta\cos\phi \end{aligned}$$

Substitution into (3.6.11) generates an ellipsoidal indicatrix (Fig. 3.11(b)), which follows the expression

$$\frac{k_x^2}{n_e^2} + \frac{k_y^2}{n_e^2} + \frac{k_z^2}{n_o^2} = \frac{\omega^2}{c^2} \tag{3.6.17}$$

This is the extraordinary indicatrix. The major and minor axes of this indicatrix are aligned to the axes of the lattice, the major axis aligned to $\hat{z}$ axis, and the axis lengths are the wavenumbers $k_{x,y,z}$ along the associated lattice axes. Equivalently, the axis lengths are the refractive indices along the lattice directions.

For either indicatrix the wavenumber is determined by the length of the k-vector at the point of intersection between that vector with the ellipsoid surface. The group velocity is the tangent to the surface at this intersection:

$$v_g = \nabla_k \omega \tag{3.6.18}$$

where $\nabla_k = \hat{k}\, \partial/\partial \mathbf{k}$. Recall that the group velocity is the result of different wavelengths travelling at different speeds. In a birefringent medium a change of k-vector at a fixed frequency is sufficient to alter the propagation speed. A perturbation analysis of Maxwell's equations (3.3.1a,b) shows the geometric interpretation. Expanding these equations to first order in $\delta\mathbf{k}$ and making the indicated dot products gives

$$\begin{aligned} \mathbf{H}^* \cdot (\delta\mathbf{k} \times \mathbf{E} + \mathbf{k} \times \delta\mathbf{E} &= \omega\delta\mathbf{B}) \\ -\mathbf{E} \cdot (\delta\mathbf{k} \times \mathbf{H}^* + \mathbf{k} \times \delta\mathbf{H}^* &= -\omega\delta\mathbf{D}^*) \end{aligned}$$

Taking the difference and applying the vector identity $\mathbf{a} \cdot (\mathbf{b} \times \mathbf{c}) = \mathbf{b} \cdot (\mathbf{c} \times \mathbf{a})$ yields

$$2\delta\mathbf{k} \cdot (\mathbf{E} \times \mathbf{H}^*) = \omega \left(\mathbf{H}^* \cdot \delta\mathbf{B} - \delta\mathbf{H}^* \cdot \mathbf{B} + \mathbf{E} \cdot \delta\mathbf{D}^* - \delta\mathbf{E} \cdot \mathbf{D}^*\right)$$

Substitution of $\mathbf{D}$ and $\mathbf{B}$ with the inverse constitutive relations (3.6.5), recognizing that $\mathbf{E} \cdot \boldsymbol{\varepsilon}^* \cdot \mathbf{E}^* = \mathbf{E}^* \cdot \boldsymbol{\varepsilon}^\dagger \cdot \mathbf{E}$ (cf. § 3.2), and applying lossless conditions $\boldsymbol{\varepsilon} = \boldsymbol{\varepsilon}^\dagger$ and $\mu = \mu^\dagger$, reduces the expansion to

$$\begin{aligned} 2\delta\mathbf{k} \cdot (\mathbf{E} \times \mathbf{H}^*) = \omega \left(\left(\mathbf{E}^* \cdot \boldsymbol{\varepsilon} \cdot \delta\mathbf{E}\right)^* - \left(\mathbf{E}^* \cdot \boldsymbol{\varepsilon} \cdot \delta\mathbf{E}\right) + \right. \\ \left. \left(\mathbf{H}^* \cdot \mu\delta\mathbf{H}\right) - \left(\mathbf{H}^* \cdot \mu\delta\mathbf{H}\right)^* \right) \end{aligned}$$

The right-hand side of (3.6.19) is an entirely imaginary quantity. As the time-averaged Poynting vector is defined as $\langle S \rangle = \Re\mathrm{e}\left(\mathbf{E} \times \mathbf{H}^*\right)/2$, this last expression is further reduced to

$$\delta\mathbf{k} \cdot \langle \mathbf{S} \rangle = 0 \tag{3.6.19}$$

Geometrically, $\langle \mathbf{S} \rangle$ is normal to the indicatrix surface at the intersection point k. As this coincides with the direction of the group velocity, is it clear that the energy flow travels at the group velocity and may not coincide with the direction of the k-vector.

3.6.2 Refraction at an Interface

Refraction and reflection at an interface between isotropic and uniaxial materials are treated nearly the same way as detailed in §3.5, but with the following modifications:

1) the *o*-ray and *e*-ray are calculated separately;
2) the effective index of the *e*-ray determines the refraction angle and reflection coefficient; and

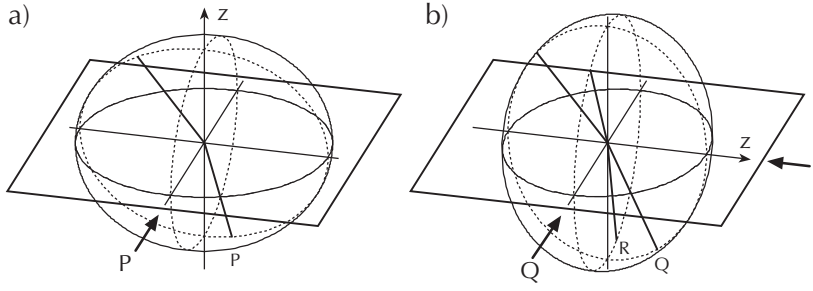

Fig. 3.12. Two orientations of the extraordinary indicatrix at a boundary. a) The $\hat{z}$ axis is normal to the interface, view P is isotropic about $\hat{z}$. b) The $\hat{z}$ axis is in the plane of the interface. Rays Q and R are orthogonal slices through the indicatrix and have different refraction angles.

3) the Poynting vector of the e-ray is not generally coincident with the k-vector and must be calculated separately.

Snell's law remains intact for birefringent materials because it enforces phase matching along the interface.

Work with birefringent crystals requires the distinction between the physical shape of the crystal and the internal orientation of the lattice. Crystal cuts can be limited by the brittleness of the material, but there are nonetheless several customary orientations that can be cut. As illustrated in Fig. 3.12, two orientations that are common are for the $\hat{z}$ normal to or lying in the interface plane. The figures illustrate the extraordinary indicatrix of a positive uniaxial crystal intersected by a plane, and rays P, Q, and R refracting into the interface.

Figure 3.12(a) illustrates the $\hat{z}$ axis cut perpendicular to the interface plane. The vertical plane defined by view P is isotropic about $\hat{z}$; the effective index of e-ray P depends only on its inclination. Figure 3.12(b) illustrates the $\hat{z}$ axis cut within the interface plane. The vertical plane defined by view Q forms an elliptical intersection with the indicatrix while the plane defined by view R forms a circle. The effective index of an e-ray refracting into a uniaxial material with this cut depends both on the inclination angle and azimuth orientation about the interface normal.

Figures 3.13(a–f) show the refractive index manifolds for views P, Q, and R for positive and negative uniaxial crystals. In each figure, the ordinary and extraordinary indicatrices are shown in plan view and bisected by the interface plane. The center of each indicatrix must lie in the plane of the interface and be located where the respective k-vector breaches the interface. As illustrated, the centers of the e- and o-indicatrices coincide.

The drawings illustrate the relative refraction for the e- and o-rays. The horizontal components of the k_e- and k_o-vectors are equal, satisfying phase matching along the interface. The e- and o-Poynting vectors are normal to

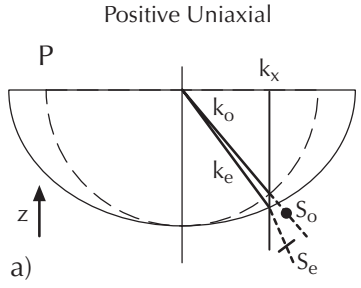

Fig. 3.13a. Refraction manifold for orientation P in a positive uniaxial crystal. Ordinary (dashed) and extraordinary (solid) indicatrices are bisected by the interface plane. Poynting vectors **S** are normal to the respective indicatrices. The *o*-ray is TE.

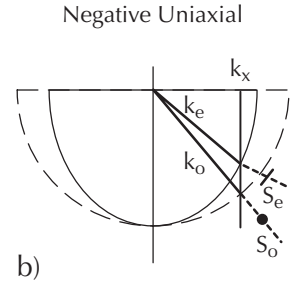

Fig. 3.13b. Refraction manifold for orientation P in a negative uniaxial crystal. Ordinary (dashed) and extraordinary (solid) indicatrices are bisected by the interface plane. Poynting vectors **S** are normal to the respective indicatrices. The *o*-ray is TE.

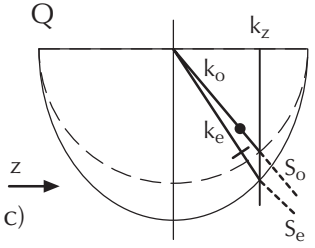

Fig. 3.13c. Refraction manifold for orientation Q. The *o*-ray is TE.

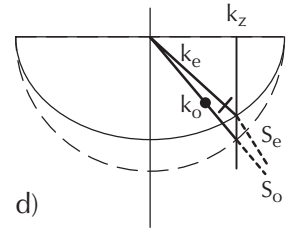

Fig. 3.13d. Refraction manifold for orientation Q. The *o*-ray is TE.

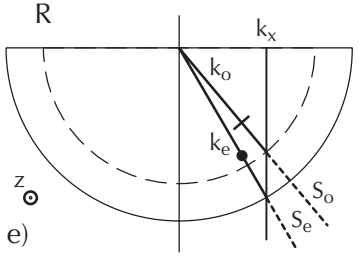

Fig. 3.13e. Refraction manifold for orientation R. The *o*-ray is TE. This is the only orientation that is isotropic for both *e*-rays and *o*-rays.

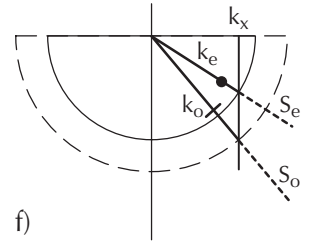

Fig. 3.13f. Refraction manifold for orientation R. The *o*-ray is TE. This is the only orientation that is isotropic for both *e*-rays and *o*-rays.

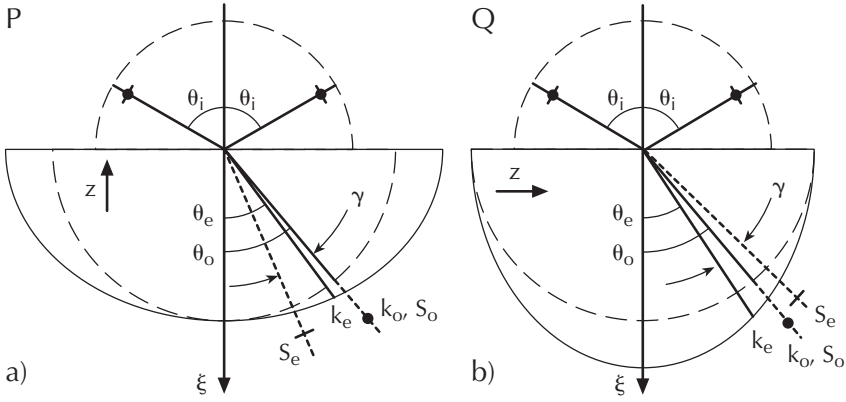

Fig. 3.14. Refraction from an isotropic material into a positive uniaxial material, views P and Q. a) Poynting vector $\mathbf{S}_e$ lies between $\mathbf{S}_o$ and $\hat{z}$. The e-ray is slow. b) Poynting vector $\mathbf{S}_e$ lies outside of $\mathbf{S}_o$. The e-ray is again slow. In both cases the o-ray is TE.

the corresponding indicatrices at the point of intersection with the respective k-vectors. The polarization orientation is also illustrated for each ray. The ordinary ray always has its polarization state perpendicular to the extraordinary axis $\hat{z}$. Depending on the direction of $\hat{z}$ at the interface, the ordinary ray may be either TE or TM. Finally, the "fast" axis is always the axis that has the lower refractive index; like TE and TM, the fast axis can be either the e- or o-ray, depending on orientation of $\hat{z}$ to the interface.

Refraction into positive uniaxial crystals for views P and Q is shown in detail in Figs. 3.14(a,b). For view P (Fig. 3.14(a)), the o-ray sees a refractive index of n_o and is TE. Snell's law determines the angle of refraction:

$$n_i \sin\theta_i = n_o \sin\theta_o \tag{3.6.20}$$

The Poynting vector $\mathbf{S}_o$ coincides with $\mathbf{k}_o$. The e-ray, which is TM, sees an effective refractive index n_{eff} given by

$$n_{\text{eff}} = \frac{n_e n_o}{\sqrt{n_e^2 \cos^2\theta_e + n_o^2 \sin^2\theta_e}} \tag{3.6.21}$$

where θ_e is the angle between $\mathbf{k}_e$ and the $\hat{z}$ axis. Snell's law then

$$n_i \sin\theta_i = n_{\text{eff}} \sin\theta_e \tag{3.6.22}$$

However, this version of Snell's law contains the angle θ_e both in n_{eff} and the sine term. Given n_e, n_o, and θ_i, (3.6.22) can be solved for θ_e:

$$\tan\theta_e = \frac{n_e}{n_o} \frac{n_i \sin\theta_i}{\sqrt{n_e^2 - n_i^2 \sin^2\theta_i^2}} \tag{3.6.23}$$

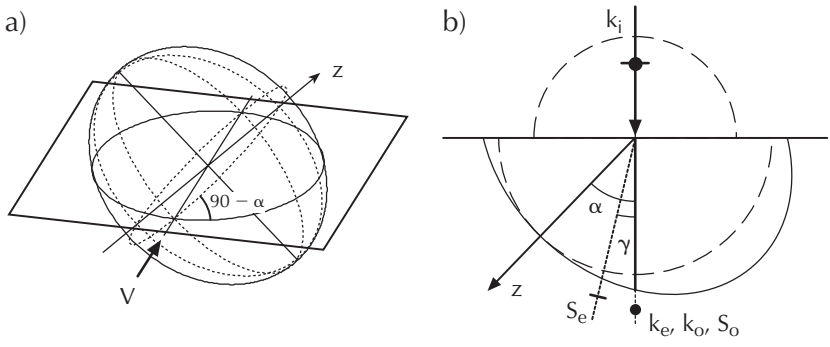

Fig. 3.15. A walkoff cut: a uniaxial crystal cut where the $\hat{z}$ axis is inclined by α from the normal. a) The (positive) extraordinary indicatrix as intersected by the interface plane. View V is indicated. b) Plan view of refraction at interface. Ordinary (dashed) and extraordinary (solid) indicatrices are shown. $\mathbf{S}_e$ is inclined by γ from the normal.

One can verify that when $n_e \to n_o$, (3.6.23) reduces to (3.6.20). The normal to the extraordinary indicatrix at the point of intersection with $\mathbf{k}_e$ determines the direction of the $\mathbf{S}_e$ vector. The angle γ between the $\mathbf{S}_o$ and $\mathbf{S}_e$ is calculated from (3.6.15) using $\theta = \theta_e$. For view P with a positive uniaxial crystal, γ is negative and $\mathbf{S}_e$ lies between $\mathbf{S}_o$ and $\hat{z}$.

View Q is for a cut such that $\hat{z}$ lies in the interface plane; this is a waveplate cut. When $\theta_i = 0$, the ordinary and extraordinary k- and Poynting vectors coincide but the refractive index of the e-ray differs from that of the o-ray. As the two rays transit the crystal, the e- and o-rays slip relative to one another, which in turn transforms the polarization state from input to output.

Figure 3.15 illustrates a third important crystal cut, the walkoff cut. A walkoff crystal is used to polarize the input light and spatially separate the resultant ordinary and extraordinary components. The crystal is cut such that its $\hat{z}$-axis is inclined from the plane of the interface. Since no walkoff occurs at 0° and 90° inclination, there is an intermediate inclination angle that maximizes the angular separation of $\mathbf{S}_e$ and $\mathbf{S}_o$.

Figure 3.15(b) illustrates the refraction manifold for an inclined-cut positive-uniaxial crystal for view V (Fig. 3.15(a)). The $\hat{z}$-axis is inclined by α with respect to the normal. When the incident light is normal to the surface, the ordinary component is not refracted and continues in the same direction. The ordinary Poynting vector runs parallel to the k_o vector. The extraordinary component, however, behaves differently. Since the input angle (as illustrated) is normal, the extraordinary k-vector also continues into the crystal without refraction and runs parallel to the k_o vector. However, the point of intersection of k_e with the extraordinary indicatrix leads to a deflected Poynting vector. The deflection for a positive-uniaxial crystal is in the direction of the $\hat{z}$ axis.

The deflection angle γ, also known as the walkoff angle, is governed by (3.6.15) with α in place of θ (note that n_e is not replaced by n_{eff}: the

deflection equation is written in terms of the cardinal indices). In order to maximize the walkoff angle γ, (3.6.15) is differentiated with respect to α and set to zero. The cut angle $\tilde{\alpha}$ that maximizes the walkoff angle is

$$\tan(\tilde{\alpha}) = \frac{n_e}{n_o} \tag{3.6.24}$$

and the corresponding deflection angle is

$$\tan(\gamma_{\max}) = -\frac{1}{2}\left(\frac{n_e}{n_o} - \frac{n_o}{n_e}\right) \tag{3.6.25}$$

The governing quantity is the ratio n_e/n_o, rather than the difference. A positive-uniaxial crystal having 10% birefringence, that is, $n_e/n_o = 1.1$, gives a maximum walkoff angle $\gamma_{\max} \simeq 5.45°$ for a cut angle of $\tilde{\alpha} \simeq 47.7°$.

A walkoff crystal makes two parallel but laterally displaced, orthogonally polarized output rays when the input ray is perpendicular to the input face, and the input and output faces are cut parallel to one another. The index of the ordinary ray is n_o, while that of the extraordinary ray is (compare (3.6.21))

$$n_{\text{eff}} = \frac{n_e n_o}{\sqrt{n_e^2 \cos^2(\theta_e + \alpha) + n_o^2 \sin^2(\theta_e + \alpha)}} \tag{3.6.26}$$

For a crystal cut at $\tilde{\alpha}$ the effective index is

$$n_{\text{eff}} = \sqrt{\frac{1}{2}\left(n_e^2 + n_o^2\right)} \tag{3.6.27}$$

This is, in fact, just the average of the permittivities along the cardinal directions.

The effective path length L_{eff} of the extraordinary ray is the length traversed by the k_e vector times the effective index. That is, the path length of $\mathbf{S}_e$ does not enter into the effective path. The path-length difference for a walkoff crystal of length L is $L_{\text{eff}} - L_o = (n_{\text{eff}} - n_o)\, L$.

3.6.3 Total Internal Reflection

Total internal reflection (TIR) for birefringent materials is more interesting than for isotropic materials because its onset differs for *e*- and *o*-rays. Otherwise, the physics of TIR remains the same as detailed in §3.5.6. This section analyzes a birefringent polarizer that uses selective TIR, and asymmetric TIR where the input and output angles are unequal.

Figure 3.16 illustrates a polarizing birefringent wedge. The $\hat{z}$ axis of the wedge is cut normal to the plane of the page and the output face is tilted by angle θ_p from the input face. The incident light is normal to the input face. Since the polarization of the *o*- and *e*-rays is perpendicular to the $\hat{z}$ axis, the Poynting vectors coincide with their respective *k*-vectors. No refraction

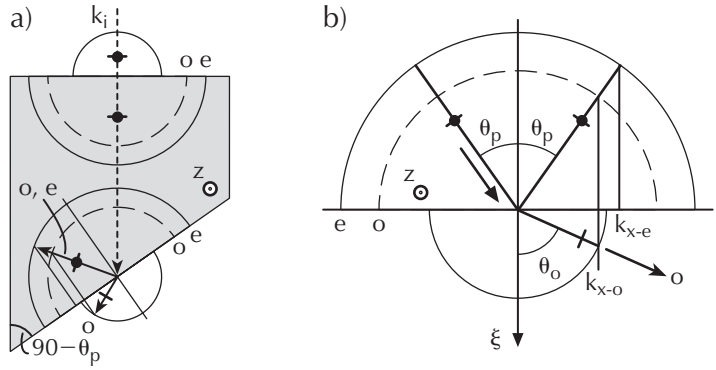

Fig. 3.16. Polarizing wedge. a) Cross-section of a polarizing birefringent wedge cut with $\hat{z}$ pointing out of the page. Only the *o*-ray survives refraction. b) Plan view of output refraction manifold.

is experienced at the input. However, the inclination of the output face cuts off transmission for the *e*-ray but not the *o*-ray. This is because the refractive indices of the two rays differ. The critical angles for the two polarizations are

$$\theta_{c,e} = \sin^{-1}(n_i/n_e)$$

for the *e*-ray and

$$\theta_{c,o} = \sin^{-1}(n_i/n_o)$$

for the *o*-ray, where n_i is the isotropic index, possibly air. As long as θ_p falls within $\theta_{c,e} \le \theta_p \le \theta_{c,o}$ then only the *o*-ray emerges from the output face. The *e*-ray experiences TIR. The angle at which the *o*-ray emerges with respect to the axis of the input ray is

$$\theta_o = \sin^{-1}\left(\frac{n_o}{n_i}\sin\theta_p\right)$$

The *o*-ray is TM at the second interface and will suffer reflection, reducing its transmission. The reflection coefficient is determined by (3.5.40). The Shirasaki prism solves this problem by setting θ_p to Brewster's angle (see §4.7.3).

Another example of the effects of birefringent total internal reflection is the asymmetric reflection created in a walkoff-cut crystal, Fig. (3.17). The left side of the figure illustrates the configuration, where the $\hat{z}$ axis is cut at angle α and the incident light is normal to the input. The *k*-vector does not refract into the crystal, but the extraordinary Poynting vector tilts upward by angle γ. The Poynting vector propagates until it hits the roof of the crystal, whereupon it experiences TIR as long as the outside refractive index is suitably low. After total internal reflection the *k*- and Poynting vectors point downward. The *k*- and Poynting vectors refract at the output surface and subsequently run parallel to one another.

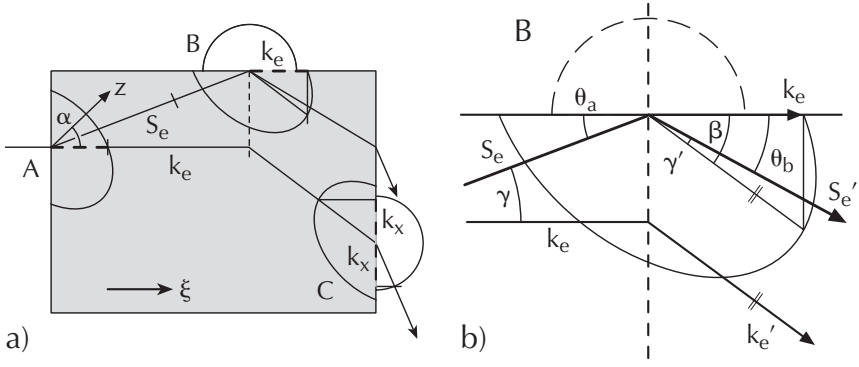

Fig. 3.17. TIR from roof of walkoff block. a) Path of e-ray k- and Poynting vectors. Position A: normal incidence, walkoff of extraordinary ray. Position B: TIR from roof, asymmetric reflection and direction change of k-vector. Position C: refraction at output. b) Detail of Position B.

Figure (3.17b) illustrates the detail of the TIR at the roof of the walkoff crystal. The extraordinary-index refraction manifold is shown tilted by angle α with respect to the roof. The incident vector $\mathbf{k}_e$ is parallel to the roof. The reflected wave must maintain phase matching along the roof, and, unlike an isotropic material, the ellipsoidal shape of the extraordinary indicatrix allows for two solutions: $\mathbf{k}_e$ that runs parallel with the roof, and $\mathbf{k}'_e$ that tilts downward at angle β. To calculate the angle β, the effective index n'_{eff} associated with $\mathbf{k}'_e$ (when projected along the horizontal axis) must match the effective index n_{eff} associated with $\mathbf{k}_e$. Thus,

$$n'_{\text{eff}} \cos\beta = n_{\text{eff}}$$

where

$$n'_{\text{eff}} = \frac{n_e n_o}{\sqrt{n_e^2 \cos^2(\alpha+\beta) + n_o^2 \sin^2(\alpha+\beta)}}$$

Solving for $\tan\beta$ gives

$$\tan\beta = \frac{2(n_e^2 - n_o^2)\sin\alpha\cos\alpha}{n_e^2 \sin^2\alpha + n_o^2 \cos^2\alpha} \tag{3.6.28}$$

The vector $\mathbf{k}'_e$ is tilted downward by angle β. The deviation angle γ' between Poynting vector $\mathbf{S}'_e$ and $\mathbf{k}'_e$ is calculated from (3.6.15), replacing θ with $\alpha+\beta$. The reflection angle θ_b with respect to the roof is $\theta_b = \beta - \gamma'$. Generally speaking, $\theta_a \neq \theta_b$, although the values can be close.

When the tilt angle is optimized for maximum walkoff, $\tan\tilde{\alpha} = n_e/n_o$. Substituting this angle into (3.6.28) gives

$$\tan\beta\,(\tilde{\alpha}) = \left(\frac{n_e}{n_o} - \frac{n_o}{n_e}\right) \tag{3.6.29}$$

For $n_e/n_o = 1.1$, $\beta \simeq 10.8°$. Another relevant identity is

$$\tan(\tilde{\alpha} + \beta(\tilde{\alpha})) = \left(\frac{n_e}{n_o}\right)^3 \tag{3.6.30}$$

Combined, the inclination of $\mathbf{S}'_e$ to $\mathbf{k}'_e$ is given by

$$\tan\gamma'(\tilde{\alpha}) = \frac{1-(n_e/n_o)^2}{1+(n_e/n_o)^4}\,\frac{n_e}{n_o} \tag{3.6.31}$$

Substitution yields $\gamma' \simeq 5.36°$. Therefore, the reflected angle is $\theta_b \simeq 5.44°$. This is compared with $\theta_a \simeq 5.45°$. Here the reflected and incident TIR angles are nearly the same. This is because $\tilde{\alpha}$ maximizes γ; at the maximum the system is stationary. Asymmetry occurs for lower walkoff angles.

3.6.4 Polarization Transformation

A waveplate is a birefringent crystal cut so that its extraordinary axis lies in the plane of the input, and the input and output crystal faces are parallel. A light ray normally incident on the input face is resolved into ordinary and extraordinary components, according to the relative orientation of the input polarization and the e-axis of the waveplate. The k- and Poynting vectors within the crystal propagate collinearly. The wavenumbers for the two components are

$$k_e = \frac{\omega}{c}\,n_e, \quad k_o = \frac{\omega}{c}\,n_o \tag{3.6.32}$$

Therefore the phase velocities differ. The difference in phase velocity results in the fast component walking through the slow component, slipping one full optical wave every birefringent beat length.

Strictly speaking, the ordinary and extraordinary waves within the waveplate propagate independently from one another, and it is accurate to say only linearly polarized fields exist. Once the fields emerge from the waveplate they continue to run collinearly but have a phase slip between them. This phase slip makes the output polarization (generally) different from the input polarization. Within a waveplate, the phase slip at any position z_o is represented by a polarization rotation *as if* the waveplate ended at z_o.

Figure 3.18 illustrates the polarization evolution along a long waveplate in laboratory coordinates and Stokes coordinates. In the laboratory frame, an input polarization state $|s\rangle$ is resolved into ordinary and extraordinary components at the input face of the waveplate. These two components have different wavelengths and travel at different phase velocities. The phase slip φ between the components is called the birefringent phase and as a function of travel distance z is defined by

$$\varphi(\omega, z) = \frac{\omega}{c}\,\Delta n z \tag{3.6.33}$$

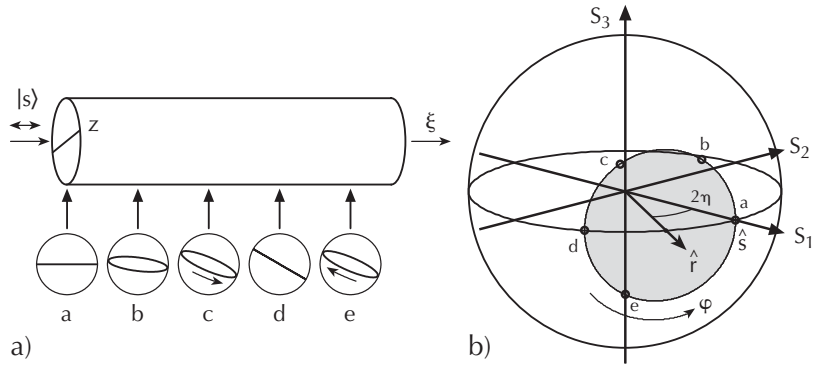

Fig. 3.18. Polarization transformation along a waveplate. a) The input SOP $|s\rangle$ is projected onto $\hat{z}$, which is tilted by angle η within the polarization plane. The projection generates two collinear waves having different wavelengths. The phase slip along the waveplate transforms the state of polarization from state a through e. b) Stokes picture of polarization change. Precession of $\hat{s}$ about $\hat{r}$.

where Δn is the birefringence $\Delta n = n_e - n_o$. The travel distance over which the components slip by one full wave is called the birefringent beat length. This distance is defined by

$$\Lambda = \frac{\lambda_0}{\Delta n} \tag{3.6.34}$$

where λ_o is the free-space wavelength. The positive uniaxial crystal YVO_4 has a birefringence of $\Delta n \simeq 0.2$; the corresponding beat length is only 7.5 μm at $\lambda_o \simeq 1.5$ μm.

The phase slip through the waveplate changes the polarization state. Figure 3.18(b) illustrates the corresponding Stokes transformation. As only the phase changes but not the power split between e- and o-components, the precession circle is traced. The birefringent axis of the waveplate lies on the equator of the Poincaré sphere. The polarization evolution is periodic with travel distance.

The birefringent phase φ also depends on frequency. The free-spectral range is the analogue to the birefringent beat length but for frequency change, not length change. However, there is an important subtly: the ordinary and extraordinary refractive indices are generally frequency dependent. To first order the refractive index n is replaced by the group index n_g. Accounting for the group index, the free-spectral range (FSR) of a waveplate of length L is defined by $\omega_2 - \omega_1 = 2\pi \times \text{FSR}$, or

$$\text{FSR} = \frac{c}{\Delta n_g L} \tag{3.6.35}$$

The free-spectral range is given in cyclic frequency. Subsection entitled, "Free-Spectral Range and Group Index" starting on page 158 details the relation between phase and group indices.

The accrual of phase slip due to frequency change is tantamount to a relative delay between the two components. This delay is called the differential group delay (DGD). As delay is defined as $\tau = \partial\varphi/\partial\omega$, the DGD for a waveplate is

$$\tau = \frac{\Delta n_g L}{c} = \frac{1}{\mathrm{FSR}} \tag{3.6.36}$$

With this definition of differential group delay, the birefringent phase as a function of frequency is written $\varphi = \omega\tau$. An output polarization state precesses about the birefringent axis (of a single homogeneous section) in Stokes space just the same as if the length changed, but in the case of length change the precession angle is $\varphi = 2\pi z/\Lambda$.

3.7 Gyrotropic Materials

Gyrotropic materials are those whose optical properties are effected by either an applied magnetic field or their own internal magnetization. In either case the eigen-axes are elliptical or circular rather than linear. Moreover, unique to gyrotropic materials is their nonreciprocal polarization rotation. This nonreciprocal rotation is due to a reorientation of the eigen-axes between forward and backward transit. The term "non-reciprocal" is of unfortunate historical origin because one typically thinks of a non-linear system being non-reciprocal. Non-reciprocity of a non-linear system means one cannot reverse time and end up with what was at the beginning. Gyrotropic processes, instead, are fully reciprocal under time reversal. Time reversal not only flips the propagation direction but also reverses the electron spin which is the source of magnetization. Non-reciprocity for gyrotropic media refers to polarization transformation for forward and backward propagation.

There are a vast array of materials and conditions that exhibit gyrotropic behavior. Gyrotropic effects are known in gases, liquids, and solids. Gyrotropic effects are also known to exist from radio-frequency through the ultraviolet. A full exposition of gyrotropy requires a quantum mechanical formalism, which is not the thrust of this text. Nonetheless, there are two steps involved when studying these materials. First, a microscopic-level analysis determines the origin and character of the gyrotropy, culminating in a constitutive relation. Second, given the constitutive relation, a kDB analysis predicts the interaction of light with the material. Common to most all gyrotropic materials is the constitutive relation of the permittivity tensor:

$$\boldsymbol{\varepsilon} = \begin{pmatrix} \varepsilon & -j\varepsilon_g & \\ j\varepsilon_g & \varepsilon & \\ & & \varepsilon_z \end{pmatrix} \tag{3.7.1}$$

The diagonal entries look like a uniaxial birefringent material. The off-diagonal entries are characteristic of gyrotropy. These entries are purely imaginary and keep the tensor $\boldsymbol{\varepsilon}$ Hermitian. For low, non-optical frequencies, the permeability tensor $\boldsymbol{\mu}$ takes the form of (3.7.1) and $\boldsymbol{\varepsilon}$ is a scalar.

3.7.1 Magnetic Material Classes

There are five classes of magnetic materials that exhibit magneto-optical effects: diamagnetic, paramagnetic, ferromagnetic, antiferromagnetic, and ferrimagnetic. Diamagnetic and paramagnetic materials have no intrinsic magnetization; these materials exhibit weak magneto-optical effects. Ferro-, antiferro- and ferrimagnetic materials do have intrinsic magnetization and their magneto-optical effects are dominated by their internal magnetization rather than an external field (unless of high coercivity). These materials can exhibit strong magneto-optical effects.

A diamagnetic material has no magnetic dipole moments at a microscopic level. Only through coercion from an external field does this material class exhibit gyrotropic behavior. The external field splits the excited-state electron levels of the constituent atoms, thereby inducing a refractive index splitting. A paramagnetic material does possess intrinsic magnetic dipole moments among some if not all of the constituent atoms. These magnetic moments exist in the ground state and tend toward cancellation on a nano-scale. An externally applied magnetic field splits the ground state, rather than the excited state, of the atoms, inducing a refractive index splitting. A finite temperature populates the upper level of the split ground state, again leading to general cancellation of the magnetization. Magneto-optical effects can be stronger in paramagnetic materials than in diamagnetic materials, but at the cost of a fall higher temperature sensitivity.

Ferro-, antiferro-, and ferrimagnetic materials are more complex. These materials all exhibit long-range spin ordering. A homogeneously ordered region is called a domain. Domains exist even in the absence of an applied magnetic field and the magnetization within a domain can be orders of magnitude stronger than for dia- or paramagnetic materials. In ferromagnetic materials, the spins of unpaired valence electrons align, generating a large magnetization within a domain. However, on a microscopic scale neighboring domains are coerced to align anti-parallel and buck a large spontaneous magnetization. An external field, however, coerces the domains to align preferentially in the direction of the applied field, which in turn induces a strong magnetic reaction to the field. In antiferromagnetic materials the spins of adjacent unpaired valence electrons anti-align and cancel. While the process of spin-orbit coupling places antiferromagnetic materials in the same category as ferromagnetic materials, magnetization of this type is weak. Finally, ferrimagnetic materials exhibit a coupling of two interstitial magnetic sublattices that couple antiferromagnetically. Generally, one sublattice has a stronger magnetization than the other, offering some degree of overall magnetization.

Ferro-, antiferro-, and ferrimagnetic materials have such strong intrinsic magnetization that their magneto-optical properties are dominated by the internal fields rather than applied fields (of a coercion order one would expect in a telecommunications environment). Often, such complex material structures require measurements of their magneto-optical properties since a

first-principles derivation is too complex. Moreover, these materials can have significant temperature dependence since thermal vibration disrupts the zero-Kelvin alignment. In fact, at zero Kelvin, the magnetization of a ferromagnet is largest, the magnetization decreases monotonically with increased temperature, and finally vanishes at the Curie temperature T_c.

In this text, a short derivation using classical electron motion is presented to motivate the construction of the constitutive relation with linear entries. Indeed, the Lorentz force is the only tool presented in this text to address the present analysis. Only diamagnetic materials yield to the Lorentz-force analysis. The reader is cautioned about adopting this derivation to other materials. Rather, references [3, 6] and the references found within provide a solid foundation on which to pursue more detailed studies of the microscopic behavior.

3.7.2 Permittivity of Diamagnetic Materials

Magnetization of diamagnetic materials is generated by an externally applied magnetic field. As discussed in §3.4, the magnetic field of an electro-magnetic wave is not strong enough to generate an appreciable force on the bound electron since $|\omega \mathbf{r}\mathbf{B}| \ll |\mathrm{e}\mathbf{E}|$. However, an external biasing field can easily influence the motion. Consider once again the bound-electron equation of motion (3.4.2) rewritten in time-harmonic form and with an external DC magnetic field aligned along $+\hat{z}$:

$$\left(-\omega^2 + \omega_o^2\right)\mathbf{r} + j\omega(\mathrm{e}/m)\left(\mathbf{r} \times B_z\right) = -(\mathrm{e}/m)\mathbf{E} \tag{3.7.2}$$

The spring-constant resonance is $\omega_o = K/m$. Before the susceptibilities are calculated, intuition can be developed by solving (3.7.2) under simplifying assumptions. Consider a ray propagating along the $+\hat{z}$ direction; in this case $\mathbf{r} \cdot \hat{z} = 0$. Separating (3.7.2) into its components and solving for $\mathbf{r}$ gives

$$\begin{pmatrix} r_x \\ r_y \end{pmatrix} = \frac{a_2}{1 - a_1^2} \begin{pmatrix} 1 & -ja_1 \\ ja_1 & 1 \end{pmatrix} \begin{pmatrix} E_x \\ E_y \end{pmatrix}$$

where $a_1 = \omega(\mathrm{e}/m)B_z/(\omega_o^2 - \omega^2)$ and $a_2 = -(\mathrm{e}/m)/(\omega_o^2 - \omega^2)$. The eigenvalue and eigenvector solutions are

$$\lambda_+ = 1 + a_1, \quad \lambda_- = 1 - a_1$$

$$\mathbf{E}_+ = \begin{pmatrix} 1 \\ j \end{pmatrix}, \quad \mathbf{E}_- = \begin{pmatrix} 1 \\ -j \end{pmatrix}$$

Counter-clockwise and clockwise polarization states of $\mathbf{E}$ are the eigenstates of the system. These two states in turn induce a circular motion of the bound electrons about the B_z field, the counter-clockwise orbit having the larger radius of the two. The circular electron trajectory is called cyclotron motion.

As the susceptibility is intimately related to the electron motion, one should expect that the eigen-polarizations of the system, when simplified in this manner, are circular and that the refractive indices are different for ccw and cw polarizations, the larger index corresponding to the larger electron radius.

Returning to the detailed analysis of susceptibilities based on the Lorentz force, recall that the polarization density is defined as $\mathbf{P} = -N\mathrm{e}\mathbf{r}$. The equation of motion (3.7.2) is recast in terms of $\mathbf{P}$ and $\mathbf{E}$:

$$\left(\omega_o^2 - \omega^2\right)\mathbf{P} + j\omega(\mathrm{e}/m)\left(\mathbf{P} \times B_z\right) = N\mathrm{e}^2/m\mathbf{E} \tag{3.7.3}$$

Expanding the curl, the cartesian components in matrix form are

$$\begin{pmatrix} \left(\omega_o^2 - \omega^2\right) & +j\omega\omega_c & 0 \\ -j\omega\omega_c & \left(\omega_o^2 - \omega^2\right) & 0 \\ 0 & 0 & \left(\omega_o^2 - \omega^2\right) \end{pmatrix} \begin{pmatrix} P_x \\ P_y \\ P_z \end{pmatrix} = \frac{N\mathrm{e}^2}{m} \begin{pmatrix} E_x \\ E_y \\ E_z \end{pmatrix}$$

where the cyclotron resonance frequency ω_c is defined as

$$\omega_c = \frac{\mathrm{e}B_z}{m} \tag{3.7.4}$$

The dielectric susceptibility tensor $\boldsymbol{\chi}_e$ relates the components of the electric field to the polarization density: $\mathbf{P} = \varepsilon_o \boldsymbol{\chi}_e \mathbf{E}$. Inverting (3.7.4) gives the components of the electric susceptibility tensor

$$\boldsymbol{\chi}_e = \begin{pmatrix} \chi_{11} & -j\chi_{12} & \\ j\chi_{12} & \chi_{11} & \\ & & \chi_{33} \end{pmatrix} \tag{3.7.5}$$

where

$$\chi_{11} = \frac{N\mathrm{e}^2}{m\varepsilon_o} \frac{\left(\omega_o^2 - \omega^2\right)}{\left(\omega_o^2 - \omega^2\right)^2 - \omega^2\omega_c^2} \tag{3.7.6a}$$

$$\chi_{12} = \frac{N\mathrm{e}^2}{m\varepsilon_o} \frac{\omega\omega_c}{\left(\omega_o^2 - \omega^2\right)^2 - \omega^2\omega_c^2} \tag{3.7.6b}$$

$$\chi_{33} = \frac{N\mathrm{e}^2}{m\varepsilon_o} \frac{1}{\left(\omega_o^2 - \omega^2\right)} \tag{3.7.6c}$$

The susceptibility χ_{12} is directly related to the strength and direction of the fixed magnetic field B_z. The susceptibility χ_{11} experiences a second-order detuning due to the field, but is generally comparable in magnitude to χ_{33} when far away from absorption resonance. The permittivity tensor $\boldsymbol{\varepsilon}$ relates to the susceptibility in the usual way: $\boldsymbol{\varepsilon} = \varepsilon_o(1 + \boldsymbol{\chi}_e)$. The entries in $\boldsymbol{\varepsilon}$ correspond to those in $\boldsymbol{\chi}_e$ by

$$\varepsilon = \varepsilon_o(1 + \chi_{11}) \tag{3.7.7a}$$

$$\varepsilon_z = \varepsilon_o(1 + \chi_{33}) \tag{3.7.7b}$$

$$\varepsilon_g = \varepsilon_o\chi_{12} \tag{3.7.7c}$$

where the subscripts z and g denote the dielectric constant along the $\hat{z}$ axis and the gyrotropic dielectric value, respectively. The impermittivity tensor $\boldsymbol{\kappa}$ required for the kDB calculations is

$$\begin{pmatrix} \varepsilon & -j\varepsilon_g & \\ j\varepsilon_g & \varepsilon & \\ & & \varepsilon_z \end{pmatrix}^{-1} = \begin{pmatrix} \kappa & j\kappa_g & \\ -j\kappa_g & \kappa & \\ & & \kappa_z \end{pmatrix} \tag{3.7.8}$$

where

$$\kappa = \frac{\varepsilon}{\varepsilon^2 - \varepsilon_g^2}, \quad \kappa_g = \frac{\varepsilon_g}{\varepsilon^2 - \varepsilon_g^2}, \quad \kappa_z = \frac{1}{\varepsilon_z} \tag{3.7.9}$$

Note from (3.7.8) that indeed $\boldsymbol{\varepsilon} = \boldsymbol{\varepsilon}^\dagger$, so the system remains ideally lossless: no work is done on the electrons due to the fixed magnetic field, all energy coupled into the cyclotron motion is recovered.

3.7.3 Propagation in Gyrotropic Materials

The constitutive relations for gyrotropic materials are

$$\mathbf{E} = \boldsymbol{\kappa} \cdot \mathbf{D}$$
$$\mathbf{H} = \mu \mathbf{B}$$

where $\boldsymbol{\kappa}$ is given by (3.7.8). Rotation into the kDB frame gives

$$\mathbf{E}_k = \boldsymbol{\kappa}_k \cdot \mathbf{D}_k \tag{3.7.10a}$$
$$\mathbf{H}_k = \mu \mathbf{B}_k \tag{3.7.10b}$$

where the transformed impermittivity tensor relation is

$$\boldsymbol{\kappa}_k = \begin{pmatrix} \kappa & j\kappa_g \cos\theta & j\kappa_g \sin\theta \\ -j\kappa_g \cos\theta & \kappa \cos^2\theta + \kappa_z \sin^2\theta & (\kappa - \kappa_z)\sin\theta\cos\theta \\ -j\kappa_g \sin\theta & (\kappa - \kappa_z)\sin\theta\cos\theta & \kappa \sin^2\theta + \kappa_z \cos^2\theta \end{pmatrix} \tag{3.7.11}$$

There is no ϕ dependence in $\boldsymbol{\kappa}$. The eigenvectors of (3.7.8) are circular in the plane perpendicular to $\hat{z}$, so $\boldsymbol{\kappa}$ is invariant to any rotation ϕ. Substitution of (3.7.11) into the coupled kDB equations (3.3.5) gives

$$\begin{pmatrix} \kappa_{11} & j\kappa_{12} \\ -j\kappa_{12} & \kappa_{22} \end{pmatrix} \begin{pmatrix} D_1 \\ D_2 \end{pmatrix} = \begin{pmatrix} 0 & u \\ -u & 0 \end{pmatrix} \begin{pmatrix} B_1 \\ B_2 \end{pmatrix} \tag{3.7.12a}$$

$$\nu \begin{pmatrix} B_1 \\ B_2 \end{pmatrix} = \begin{pmatrix} 0 & -u \\ u & 0 \end{pmatrix} \begin{pmatrix} D_1 \\ D_2 \end{pmatrix} \tag{3.7.12b}$$

where

$$\kappa_{11} = \kappa, \quad \kappa_{12} = \kappa_g \cos\theta, \quad \text{and} \quad \kappa_{22} = \kappa \cos^2\theta + \kappa_z \sin^2\theta$$

Elimination of **B** generates the governing equation

$$\begin{pmatrix} (u^2/\nu - \kappa) & -j\kappa_g \cos\theta \\ j\kappa_g \cos\theta & (u^2/\nu - \kappa) + (\kappa - \kappa_z)\sin^2\theta \end{pmatrix} \begin{pmatrix} D_1 \\ D_2 \end{pmatrix} = 0 \tag{3.7.13}$$

Notice that the sign of the off-diagonal elements changes with $\theta + \pi$: reversal of propagation direction generates a transposition of the eigenvectors. More on this to follow.

In order to arrive at a compact expression for the eigenvectors and eigenvalues, (3.7.13) is first rearranged to the form

$$\begin{pmatrix} p & -jq \\ jq & p+2 \end{pmatrix} \begin{pmatrix} D_1 \\ D_2 \end{pmatrix} = 0 \tag{3.7.14}$$

where

$$p = \frac{2(u^2/\nu - \kappa)}{(\kappa - \kappa_z)\sin^2\theta}, \qquad q = \frac{2\kappa_g \cos\theta}{(\kappa - \kappa_z)\sin^2\theta}$$

The eigenvectors and corresponding eigenvalues of (3.7.14) are

$$|r_\pm\rangle = \frac{1}{\sqrt{2(1 + q^2 \pm \sqrt{1+q^2})}} \begin{pmatrix} q \\ j(1 \pm \sqrt{1+q^2}) \end{pmatrix} \tag{3.7.15}$$

and

$$p_\pm + 1 \pm \sqrt{1+q^2} = 0 \tag{3.7.16}$$

The gyrotropic angle ψ is defined as

$$\tan 2\psi = \frac{2\kappa_g \cos\theta}{(\kappa - \kappa_z)\sin^2\theta} \tag{3.7.17}$$

Identifying the gyrotropic angle with (3.7.15), the eigenvectors are expressed in the more revealing form:

$$|r_+\rangle = \begin{pmatrix} \sin\psi \\ j\cos\psi \end{pmatrix}, \quad |r_-\rangle = \begin{pmatrix} \cos\psi \\ -j\sin\psi \end{pmatrix}$$

In Stokes space the eigenvectors are

$$\hat{r}_+ = \begin{pmatrix} -\cos 2\psi \\ 0 \\ \sin 2\psi \end{pmatrix}, \quad \hat{r}_- = \begin{pmatrix} \cos 2\psi \\ 0 \\ -\sin 2\psi \end{pmatrix}$$

The eigenvectors of (3.7.13) correspond to polarization states that can propagate through the gyrotropic medium without change. The eigenstates of polarization are elliptical and the ellipsoid axes in the laboratory frame are aligned

to the horizontal and vertical. The eccentricity depends on the gyrotropic angle ψ, which in turn depends on the propagation direction, wavelength, and strength of the applied magnetic field. In contrast to birefringent materials where the eigen-polarizations are linear, gyrotropic materials can have any eigen-polarization along a line of longitude through S_1. An input polarization state is resolved onto the two eigen-polarization states and in general the two states propagate with different phase velocities and energy-flow directions.

The phase-velocity eigenvalues of (3.7.13) are

$$u_{\pm}^2 = \nu\kappa_o\kappa_{\pm} \tag{3.7.18}$$

where $\varepsilon_o = 1/\kappa_o$ and

$$\kappa_{\pm} = \frac{\kappa}{\kappa_o} - \frac{(\kappa - \kappa_z)\sin^2\theta}{2\kappa_o}\left[1 \pm \sqrt{1 + \left(\frac{2\kappa_g\cos\theta}{(\kappa - \kappa_z)\sin^2\theta}\right)^2}\right] \tag{3.7.19}$$

The dispersion relations are therefore

$$k_{\pm} = \frac{\omega}{c}\frac{1}{\sqrt{\kappa_{\pm}}} \tag{3.7.20}$$

It follows that the effective refractive indices are $n_{\pm} = 1/\sqrt{\kappa_{\pm}}$. Heuristically, the refractive index has the form $n_{\pm} = n_o - \delta n \pm \delta n_g$, where n_o is the intrinsic refractive index, δn is a field-induced diminution of n_o, and δn_g is the splitting factor due to the cyclotron motion of the bound electrons.

Like birefringent media, the Poynting vectors in gyrotropic media do not necessarily align with the k-vectors of the eigenstates. Inserting (3.7.11) into (3.7.10) and remembering that $D_3 = 0$, the fields and flux densities are

$$\begin{aligned}
\mathbf{D}_k &= \hat{e}_1 D_1 + \hat{e}_2 D_2, \\
\mathbf{E}_k &= \hat{e}_1\left(\kappa_{11}D_1 + \kappa_{12}D_2\right) + \hat{e}_2\left(\kappa_{21}D_1 + \kappa_{22}D_2\right) + \\
&\qquad \hat{e}_3\left(\kappa_{31}D_1 + \kappa_{32}D_2\right), \\
\mathbf{B}_k &= u/\nu\left(-\hat{e}_1 D_2 + \hat{e}_2 D_1\right), \\
\mathbf{H}_k &= u\left(-\hat{e}_1 D_2 + \hat{e}_2 D_1\right),
\end{aligned}$$

The Poynting vector is therefore

$$\mathbf{S}_k = -\hat{e}_1 E_3 H_2^* + \hat{e}_2 E_3 H_1^* + \hat{e}_3\left(E_1 H_2^* - E_2 H_1^*\right) \tag{3.7.21}$$

The Poynting vector is generally not aligned to the k-vector. In contrast to birefringent materials, the gyrotropic Poynting vector is tilted away from the k-vector along both the $\hat{e}_1$ and $\hat{e}_2$ axes, and out of the plane of $\mathbf{k}$ and $\hat{z}$. Only when $E_3 = 0$ does the Poynting vector align with the k-vector. The E_3 field component is

$$E_3 = j\kappa_g \sin\theta D_1 + (\kappa - \kappa_z)\sin\theta\cos\theta D_2$$

which shows that $E_3 = 0$ only when either $B_z = 0$ and/or $\sin\theta = 0$. Since $B_z \neq 0$ by design, the Poynting vector aligns with the k-vector only when the propagation direction is aligned with or counter to the magnetic field direction.

3.7.4 Faraday Rotation

Applications of gyrotropic materials in telecommunication components are generally limited to applications where the Poynting vector aligns with the k-vector. In the presence of a magnetic field, this is only possible when $\sin\theta = 0$. The polarization-transforming effect that is induced when a ray travels along the $\pm\hat{z}$ direction is called Faraday rotation. As detailed below, Faraday rotation is a nonreciprocal polarization rotation. The absence of reciprocity enables key components such as isolators and circulators to be realized.

The following analysis details propagation in the $+\hat{z}$ and $-\hat{z}$ directions. Since the signs will quickly become difficult to track, the analysis is divided into a first section that details $\theta = 0$ propagation and a second section that details $\theta = \pi$ propagation.

When $\theta = 0$, the ray travels along the $+\hat{z}$ direction. The governing equation (3.7.13) simplifies to

$$\begin{pmatrix} u^2 - \nu\kappa & -j\nu\kappa_g \\ j\nu\kappa_g & u^2 - \nu\kappa \end{pmatrix} \begin{pmatrix} D_1 \\ D_2 \end{pmatrix} = 0 \tag{3.7.22}$$

The gyrotropic angle ψ, as determined by (3.7.17), is

$$\psi = \pi/4$$

The eigenvectors of forward propagation are therefore

$$|r_+\rangle = \frac{1}{\sqrt{2}} \begin{pmatrix} 1 \\ j \end{pmatrix}, \quad |r_-\rangle = \frac{1}{\sqrt{2}} \begin{pmatrix} 1 \\ -j \end{pmatrix} \tag{3.7.23}$$

The eigenvectors of the system are circular polarization states. The precession axis $\hat{r}$ in Stokes space for the forward propagation direction is $\hat{r} = +S_3$. The circular eigenstates of polarization are reminiscent of the circular electron orbital motion that was calculated at the beginning of §3.7.2. It should be no surprise that the cyclotron electron motion produces circular eigenpolarization states.

The phase-velocity eigenvalues of the system are

$$u_\pm = \sqrt{\nu(\kappa \mp \kappa_g)} \tag{3.7.24}$$

The wavenumbers and effective indices are found by substituting $u = \omega/k$, $\nu = 1/\mu_o$, and (3.7.9) for the impermittivities. The wavenumbers are

$$k_{\pm} = \frac{\omega}{c}\sqrt{\frac{\varepsilon_r^2 - \varepsilon_{gr}^2}{\varepsilon_r \mp \varepsilon_{gr}}} \tag{3.7.25}$$

where $\varepsilon_r = \varepsilon/\varepsilon_o$ and $\varepsilon_{gr} = \varepsilon_g/\varepsilon_o$. In terms of susceptibility, the wavenumbers are

$$k_{\pm} = \frac{\omega}{c}\sqrt{1 + \chi_{11} \pm \chi_{12}} \tag{3.7.26}$$

The gyrotropic effect splits the intrinsic susceptibility by $\pm\chi_{12}$.

Since the $+\hat{z}$ propagation of the ray keeps the Poynting vectors aligned with the k-vectors, and further assuming normal incidence onto the gyrotropic medium to ensure alignment of the k-vectors, the polarization state of an incident ray is resolved into right- and left-circular components which co-propagate through the medium with different phase velocities. The circular basis of the eigenmodes makes the polarization state transform along a line of latitude on the Poincaré sphere. Indeed, Table 2.1 on page 67 shows that for an eigenvector that points to $+S_3$, the transformation matrix U is

$$U = \begin{pmatrix} \cos(\varphi/2) & -\sin(\varphi/2) \\ \sin(\varphi/2) & \cos(\varphi/2) \end{pmatrix} \tag{3.7.27}$$

where the birefringent phase is defined as usual:

$$\varphi = (k_+ - k_-)z \tag{3.7.28}$$

U rotates an input state of polarization about the $+S_3$ axis by angle φ and the rotation direction is right-handed. This rotation is illustrated in Fig. 3.19(a).

The contour traced by $-\pi \le \varphi \le \pi$ is a line of constant latitude. Recall from §1.4 that a family of polarization states on a line of latitude has constant ellipticity and handedness. It is the tilt of the major axis that rotates with longitude. In the laboratory frame, the effect of Faraday rotation is to rotate the major axis of the input polarization ellipse by angle $(\varphi/2)$.

Next, consider when $\theta = \pi$; the ray travels along the $-\hat{z}$ direction while the magnetic field still points in the $+\hat{z}$ direction. The governing equation (3.7.13) simplifies to

$$\begin{pmatrix} u^2 - \nu\kappa & j\nu\kappa_g \\ -j\nu\kappa_g & u^2 - \nu\kappa \end{pmatrix} \begin{pmatrix} D_1 \\ D_2 \end{pmatrix} = 0 \tag{3.7.29}$$

The gyrotropic angle ψ, as determined by (3.7.17), is

$$\psi = -\pi/4$$

The eigenvectors of backward propagation are therefore

$$|r_+\rangle = \frac{1}{\sqrt{2}}\begin{pmatrix} 1 \\ -j \end{pmatrix}, \quad |r_-\rangle = \frac{1}{\sqrt{2}}\begin{pmatrix} 1 \\ j \end{pmatrix} \tag{3.7.30}$$

with corresponding eigenvalues

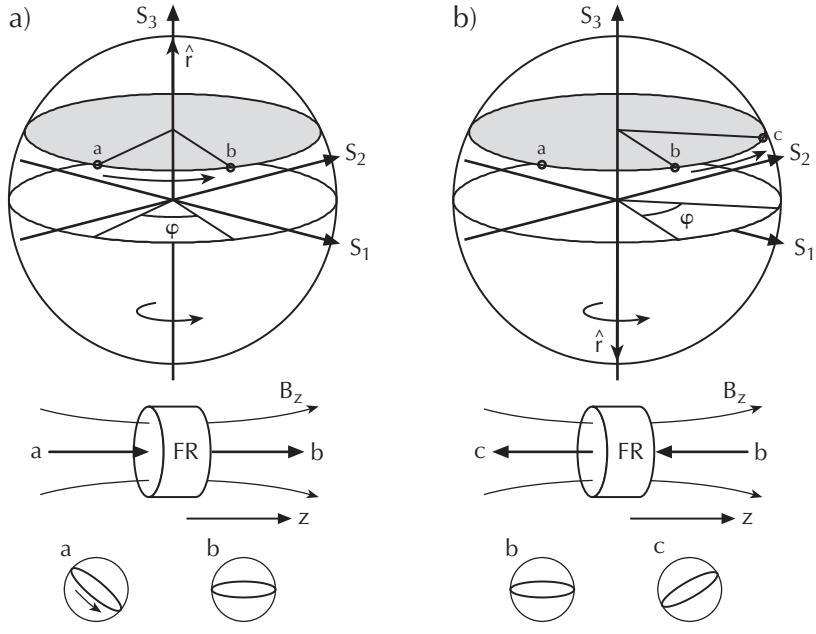

Fig. 3.19. Nonreciprocal polarization transformation via Faraday rotation. a) Forward propagation along the direction of the fixed magnetic field. Input polarization (a) right-hand precesses about $+S_3$ by φ to state (b). b) Backward propagation against the direction of the magnetic field. Polarization state (b) left-hand precesses about $-S_3$ by $|\varphi|$ to state (c).

$$u_{\pm} = \sqrt{\nu(\kappa \mp \kappa_g)} \tag{3.7.31}$$

In comparison with (3.7.23-3.7.24), the eigenvectors for backward propagation have flipped sign, while the eigenvalues remain unchanged. Rather than precessing about the $+S_3$ axis, the polarization state of a ray travelling backward precesses about the $-S_3$ axis. The transformation matrix U for backward propagation is

$$U = \begin{pmatrix} \cos(\varphi/2) & \sin(\varphi/2) \\ -\sin(\varphi/2) & \cos(\varphi/2) \end{pmatrix} \tag{3.7.32}$$

where φ is defined by (3.7.28).

The off-diagonal sign of U has changed in comparison with (3.7.27) because of precession about $-S_3$. However, the precession expression remains the same. Since precession increases with forward travel and decreases with backward travel, the net result of the backward polarization rotation is a left-hand rotation about $-S_3$ by $|\varphi|$. Figure 3.19(b) illustrates this.

The analyses for $\pm\hat{z}$ propagation show that polarization states are transformed via right-hand-rule rotation about $+S_3$ for forward and backward

propagation. Regardless of travel direction, the polarization state precesses in the same direction in Stokes space. This is completely different behavior in comparison with a optical activity (covered in the following section), where a polarization transformation due to forward travel is undone by backward travel.

The nonreciprocal character of Faraday rotation is not tantamount to violation of time reversibility. Time reversal would change the spin direction of the electrons that generate the fixed magnetic field, in addition to mapping ccw to cw circular polarizations and vica-versa. All polarization transformations induced by Faraday rotation would be undone under time reversal.

At this point it is almost trivial to point out that when the input polarization state is linear, the output state is also linear but with its major axis rotated by the medium. This behavior is the basis for all telecommunications-grade Faraday rotators. As a rule, when the input polarization is a linear state, the output state is the orthogonal linear state after $\varphi = \pi$ rotation. There is some confusion in the literature that Faraday rotation magically drives *any* input state to its orthogonal state. This analysis has shown the invalidity of such a view.

For linear input polarizations, the Faraday angle θ_F is defined as

$$\theta_F = \varphi/2 \tag{3.7.33}$$

The rotation angle θ_F is the physical, not Stokes, rotation of the linear state. The physical Faraday angle θ_F is an important quantity when considering isolator and circulator designs because this angle determines the relative orientation between two polarizers.

3.7.5 The Verdet Constant

Considering that an external magnetic field is not necessarily uniform throughout the diamagnetic medium, the overall retardation from one end to the other is

$$\varphi = \int_0^L (k_+ - k_-)\, dz$$

In the transparency regime, the wavenumbers are related to the refractive indices in the usual way: $k_\pm = wn_\pm/c$. The splitting of the refractive index for small χ_{12} in light of (3.7.26) is

$$n_+ - n_- = \frac{\chi_{12}}{\sqrt{1+\chi_{11}}} \tag{3.7.34}$$

The denominator is approximately the intrinsic refractive index to the same degree of approximation. Referring to (3.7.7a), the average refractive index is $n \simeq \sqrt{1+\chi_{11}}$, or

$$n^2 = 1 + \frac{N\mathrm{e}^2}{m\varepsilon_o}\frac{1}{\omega_o^2 - \omega^2}$$

A small susceptibility χ_{12} occurs when the cyclotron resonance frequency follows $\omega\omega_c \ll (\omega_o^2 - \omega^2)$. Inserting this condition into (3.7.7b) eliminates the susceptibility terms from (3.7.34):

$$n_+ - n_- \simeq \frac{N\mathrm{e}^3 B_z}{nm^2\varepsilon_o} \frac{\omega}{(\omega_o^2 - \omega^2)^2} \tag{3.7.35}$$

The refractive index splitting is also related to the dispersion of the intrinsic index $dn/d\lambda$ by

$$n_+ - n_- \simeq -\frac{\lambda^2 \mathrm{e}}{2\pi cm} \left(\frac{dn}{d\lambda}\right) B_z$$

Putting all of this together, the functional form of the Faraday rotation angle is

$$\theta_F = V \int_0^L B_z dz \tag{3.7.36}$$

where the Verdet constant is identified as

$$V = -\frac{\mathrm{e}\lambda}{2mc} \left(\frac{dn}{d\lambda}\right) \tag{3.7.37}$$

This expression is known as the Becquerel formula of the Verdet constant [3]. The negative sign is cancelled out by $dn/d\lambda$ for usual dispersions. The Verdet constant measures the rotary power of a material and can be used as a point of comparison between different materials. In SI units, the Verdet constant is measured in (rad/(m T)).

Fundamentally, the Verdet constant is a function of frequency and varies only to second order with the magnetic field strength. Generally is it well documented that the Verdet constant has a λ^{-2} wavelength dependence, as indicated in (3.7.35) [9]. Akin with the study of refractive index and material susceptibility, the Verdet constant of (3.7.37) is based here on a single oscillator model. More complicated materials may have multiple contributions to the Verdet constant, and the Verdet constant can certainly go negative.

3.7.6 Faraday Rotation in Ferrous Materials

The preceding analysis of diamagnetic materials resulted in an equation that linearly relates the Faraday rotation angle θ_F to the applied magnetic field B_z (cf. (3.7.36)). However, the Verdet constant for diamagnetic materials is too weak to find useful applications in telecommunications. In order to achieve a compact size the magnetization must be strong. Rare-earth iron garnets are ferrimagnetic materials that have orders of magnitude stronger rotary power than the best diamagnetic materials for the same applied magnetic field.

As outlined in §3.7.1, ferro-, antiferro-, and ferrimagnetic materials exhibit domain structure on a microscopic scale, where the magnetization within a domain is uniform and the domains spontaneously orient to prevent a large

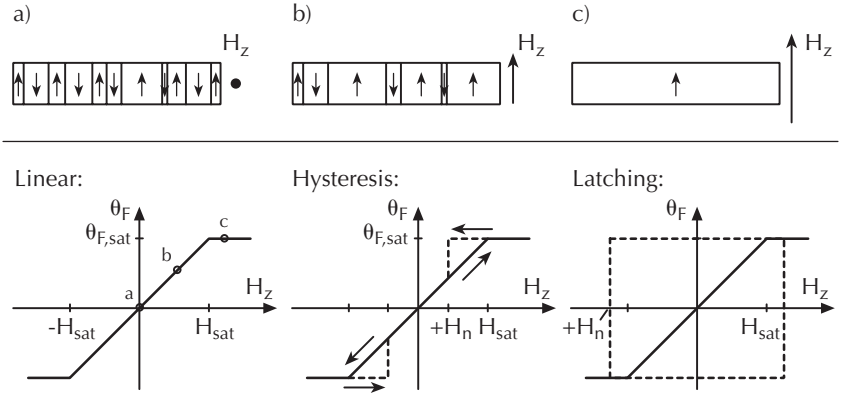

Fig. 3.20. Illustration of domain structure and alignment with applied external field. a) A demagnetized ferrimagnet: equal number of spin-up and spin-down domains. b) Partially magnetized material; some spin-down domains remain. c) Saturated material; a single spin-up domain spans the material. Below, saturation curves of θ_F vs. H_z: linear, hysteretic, and latching [14, 15].

constructive magnetic field (at least at high enough temperatures or in a demagnetized sample). In the presence of an external magnetic field the domains reorient preferentially along the field lines. However, unlike diamagnetic materials where the magnetization linearly tracks the applied field strength, all materials with domain structures saturate once a sufficiently strong field is applied. Saturation occurs when the domain boundaries are pushed to the edges of the material and only a single, unidirectional domain is left. No further magnetization occurs with increased applied field. Moreover, all magneto-optical effects are dominated by the internal magnetization rather than the applied field.

Figure 3.20 illustrates domain alignment and various magnetization curves. Figures 3.20(a–c) illustrate a demagnetized ferrimagnet having equal number of spin-up and spin-down domains (a), a partially magnetized ferrimagnet where spin-up domains expand at the expense of spin-down domains (b), and a saturated ferrimagnet where a single aligned domain spans the materials. Beyond the saturation field $H_{\rm sat}$ there is no further magnetization of the material.

The magnetization curves in the lower half of Fig. 3.20 illustrate three types of material responses. A linear magnetization curve has a one-to-one correspondence between H_z and θ_F; above $H_{\rm sat}$ angle θ_F is no longer responsive and remains fixed at $\theta_{F,\rm sat}$. A hysteretic magnetization curve is one where the magnetization, or equivalently the Faraday rotation angle θ_F, traces one path for increasing H_z and a separate path for decreasing H_z. In particular, once the applied field exceeds the the saturation field, θ_F remains fixed at $\theta_{F,\rm sat}$ until the applied field goes below the nucleation field $H_{\rm nuc}$. The nucle-

ation field is the field strength where internal fields coerce a fracturing of the single domain to reduce the potential energy of the system. A latching magnetization curve has particular interest for component applications because once the saturation field is applied, the Faraday rotation remains at $\theta_{F,\mathrm{sat}}$ even for zero external field.

When the Faraday rotation can saturate, the Verdet constant is no longer a reasonable measure since, by definition, the Verdet constant is the constant of proportionality between field and rotation. Instead, the specific rotation θ'_F is defined as

$$\theta'_F = \frac{\theta_{F,\mathrm{sat}}}{L} \tag{3.7.38}$$

or the saturation rotation $\theta_{F,\mathrm{sat}}$ per unit length. The specific rotation has units of (rad/m) [3].

In order for a ferrimagnet such as iron garnet to work well as a Faraday rotator it must be saturated. A demagnetized or partially magnetized element scatters light to an unacceptable degree. The light is scattered because the domains locally impart a polarization rotation, but the domains have no coherence or alignment. A radiation field with numerous k-vectors and polarization components must be constructed to match the boundary condition of the scattered light on the output face of the element.

That the ferrimagnet must operate in saturation is certainly a benefit because sensitivity to the applied field strength is eliminated. Without this built-in nonlinearity, much care would have to go into designing an external magnetic field that is highly uniform throughout the volume. A calculation of the magnetic field profile generated by a toroidal magnetic is given in Appendix B. Moreover, the saturation nonlinearity aids with the stringent aging requirements of all telecommunication components since the fixed magnet will degrade over time and still, with proper design, exceed the saturation field. A key design goal for an iron garnet is to have a low saturation field so that the requisite magnet can be small.

The remaining factors that must be accounted for when using iron garnets are the temperature sensitivity and wavelength variation of the specific rotation $\theta'_F(T, \lambda)$, and the wavelength dependence of the element [13–15].

3.8 Optically Active Materials

Materials that are chiral exhibit optical activity. A chiral material is one where the crystalline unit cell, or the molecular structure, differs from its mirror image; that is, the molecules have twist. A chiral molecule and its mirror image are called isomers. Most organic molecules are chiral, including sugar and DNA. For example, dextrose is right-handed sugar and fructose is left-handed sugar.

Chiral materials have a different radiation response to an optical field because nearest-neighbor dipole polarizations add constructively because of the

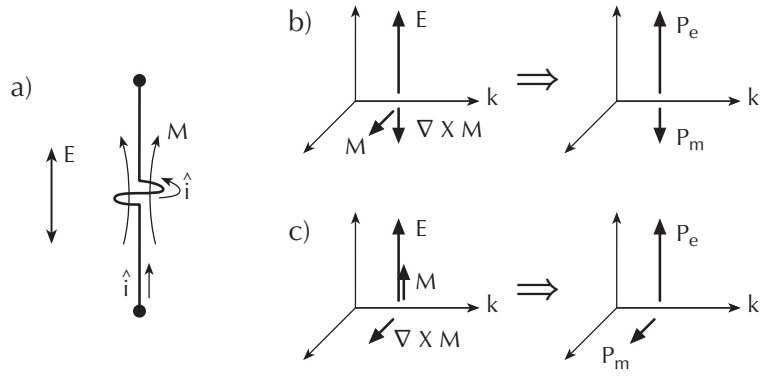

Fig. 3.21. Simple model of chiral molecular and induced polarization components [7]. a) Perfectly conducting wire of length ℓ with right-handed single turn. The applied electric field $\mathbf{E}$ induces current i, which generates both an electric polarization component $\mathbf{P}$ and a parallel magnetization component $\mathbf{M}$. b) An achiral material. $\mathbf{M}$ is perpendicular to $\mathbf{E}$ ($\mathbf{M} \parallel \mathbf{H}$), so magnetically induced polarization component $\mathbf{P}_m$ is parallel to $\mathbf{P}_e$ and makes an insignificant contribution. c) A chiral material. By construction, $\mathbf{M}$ is parallel to $\mathbf{E}$, generating magnetization contribution $\mathbf{P}_m$ perpendicular to $\mathbf{P}_e$. This one-sided persistent bias rotates the polarization state of the propagating wave.

molecular twist. The symmetry of isotropic and anisotropic materials cancels all nearest-neighbor dipole contributions, which is why they were ignored in the preceding sections. The twist of chiral materials induces both electric and magnetic dipole responses to an external electric field; these coupled responses cause optical activity.

Optical activity causes the right-hand or left-hand rotation of a linear polarization state as it propagates through the medium. A material that induces right-hand polarization rotation is called dextrorotatory and a material that induces left-hand rotation is called levorotatory. There is no *a priori* relation between the handedness of an isomer and dextro- or levo-rotatory behavior. However, if a right-handed isomer is dextrorotary, then its left-handed counterpart will be levorotatory.

The microscopic origins of optical activity can vary widely depending on the nature of the molecular or atomic structure. Optically active materials can be either reciprocal or non-reciprocal, bi-isotropic or bianisotropic, lossless or lossy. The constitutive relations differentiate these possible conditions. The common theme underlying optical activity is a coupling of the magnetic field to the electric polarizability, and the electric field to the magnetic polarizability. As an example, consider a perfectly conducting wire of length ℓ having a single spiral turn half-way along its length (Fig. 3.21(a)). When an external electric field generates a current that oscillates up and down along the wire, the current through the turn generates a magnetic flux in the direction of

the electric field. The external electric field thus elicits a collinear electric and magnetic response.

The handedness of the spiral turn determines whether the magnetic response is parallel or antiparallel with the electric response. Moreover, flipping the wire upside-down does not change the wire's handedness; handedness is an inherent property of the wire structure.

To pursue this example further, Hagan [7] considers Maxwell's equations in the absence of a current source:

$$\nabla \times \mathbf{E} = -\frac{\partial}{\partial t}(\mu_o \mathbf{H} + \mu_o \mathbf{M}) \tag{3.8.1a}$$

$$\nabla \times \mathbf{H} = \frac{\partial}{\partial t}(\varepsilon_o \mathbf{E} + \mathbf{P}) \tag{3.8.1b}$$

In a charge-free region, the divergence of the electric field is zero. Rewriting in time-harmonic form and using the vector identity $\nabla \times \nabla \times = \nabla(\nabla \cdot) - \nabla^2$ gives

$$\nabla^2 \mathbf{E} = -\omega^2 \mu_o \mathbf{P}_{\text{eff}} \tag{3.8.2}$$

where an effective polarization density $\mathbf{P}_{\text{eff}}$ is identified as

$$\mathbf{P}_{\text{eff}} = \left(\varepsilon \mathbf{E} - \frac{j}{\omega} \nabla \times \mathbf{M}\right) \tag{3.8.3a}$$

$$= \mathbf{P}_e + \mathbf{P}_m \tag{3.8.3b}$$

The polarization of the medium has two contributors: $\mathbf{P}_e$ associated with the linear dielectric and $\mathbf{P}_m$ associated with the curl of the induced magnetic flux. In achiral materials $\mathbf{E} \cdot \mathbf{H} = 0$, so the curl of the magnetic flux $(\nabla \times \mathbf{M})$ is parallel or antiparallel with the polarization $\mathbf{P}_e$. Since generally $|\varepsilon \mathbf{E}| >> |\mathbf{M}/c|$, the $\mathbf{P}_m$ contribution is negligible. However, in chiral materials, the $\mathbf{P}_m$ component lies perpendicular to $\mathbf{P}_e$. That is, since a component of $\mathbf{M}$ is generated parallel with $\mathbf{E}$, $\nabla \times \mathbf{M}$ lies perpendicular. It is the $\mathbf{P}_m$ component that distinguishes optical activity from other processes.

In order to analyze this further, the magnetization must be related to the electric field. The canonical constitutive relation between $\mathbf{M}$ and $\mathbf{H}$ is

$$\mathbf{M} = \chi_m \mathbf{H} \tag{3.8.4}$$

Now, given the particular geometry of the wire with embedded loop, the magnetic flux generated by current flow through the loop is parallel to the applied field. Moreover, the current lags the voltage due to the loop inductance. With these considerations, (3.8.4) can be rewritten as

$$\mathbf{M} = \pm j \chi_m |\mathbf{H}| \hat{\mathbf{E}} \tag{3.8.5}$$

where $|\mathbf{H}|$ is the magnitude of the magnetic field and $\hat{\mathbf{E}}$ is the direction of the electric field. The $\pm$ sign accounts for the handedness of the loop, $(-)$ for

a right-hand loop and (+) for a left-hand loop. From (3.8.1b), the magnetic field magnitude is

$$|\mathbf{H}| = \frac{\omega}{k}\left|\varepsilon\mathbf{E} - \frac{j}{\omega}\nabla\times\mathbf{M}\right| \tag{3.8.6}$$

Since $\varepsilon\mathbf{E}$ dominates the right-hand side magnitude, the curl term is neglected. The curl of $\mathbf{M}$ in (3.8.5) is then just

$$\nabla\times\mathbf{M} \simeq \pm j\chi_m\frac{\omega\varepsilon}{k}\,\nabla\times\mathbf{E} \tag{3.8.7}$$

The effective polarization density is therefore

$$\mathbf{P}_{\text{eff}} = \varepsilon\mathbf{E} + \varepsilon\beta\nabla\times\mathbf{E} \tag{3.8.8}$$

where the chirality parameter is defined as $\beta = \pm\chi_m/k$. The sign of the chirality parameter β designates the handedness, and the units of β are length. The constitutive relation between $\mathbf{D}$ and $\mathbf{E}$ are therefore

$$\mathbf{D} = \varepsilon_{\text{DBF}}\left(\mathbf{E} + \beta\nabla\times\mathbf{E}\right) \tag{3.8.9}$$

This is the Drude-Born-Fedorov constitutive relation for reciprocal chiral material. Detailed investigation of conservation of energy [4] requires a complimentary constitutive relation for the magnetic flux vector,

$$\mathbf{B} = \mu_{\text{DBF}}\left(\mathbf{H} + \beta\nabla\times\mathbf{H}\right) \tag{3.8.10}$$

The notation of ε_{DBF} and μ_{DBF} follows from [12] and is used to distinguish these values when compared to more general forms of the constitutive relations. Of immediate importance is the existence of $\nabla\times$ terms in the constitutive relations. The ∇ part is a spatial derivative, which physically means that neighboring fields contribute to the polarization. The cross in $\nabla\times$ indicates that the neighboring field contributions are perpendicular to the applied field. The presence of the $\nabla\times$ terms in (3.8.9-3.8.10) generates a persistent bias perpendicular to the propagation direction which rotates the fields in a circular motion. Circular states of polarization are in fact the eigenstates of optical activity.

The above derivation is heuristic but not particularly rigorous. More sophisticated calculations start with dipole-dipole interactions within chiral molecules and proceed to generate coupled equations of bound-electron motion. From these the spatially averaged polarization and magnetization vectors are derived [2]. While telecommunications applications rarely require more detailed knowledge, bio-optics is replete with applications of molecular mechanics and optical activity. The interested reader is referred to [1, 2, 12].

3.8.1 Propagation in Bi-Isotropic Media

The most general constitutive relations for bi-isotropic optically active media are [12]

$$\mathbf{D} = \varepsilon\mathbf{E} + (\chi_{\mathrm{T}} - j\kappa_{\mathrm{P}})\sqrt{\mu_o\varepsilon_o}\,\mathbf{H} \tag{3.8.11a}$$

$$\mathbf{B} = \mu\mathbf{H} + (\chi_{\mathrm{T}} + j\kappa_{\mathrm{P}})\sqrt{\mu_o\varepsilon_o}\,\mathbf{E} \tag{3.8.11b}$$

where χ_{T} is the Tellegen magnetoelectric parameter and κ_{P} is the Pasteur chirality parameter. When $\chi_{\mathrm{T}} \neq 0$ the medium is non-reciprocal. When $\kappa_{\mathrm{P}} \neq 0$ the medium is chiral. Either or both terms can be non-zero. The constitutive relations (3.8.11) follow from (3.8.9-3.8.10) for a proper association of constants $(\varepsilon_{\mathrm{DBF}}, \mu_{\mathrm{DBF}}, \beta) \to (\varepsilon, \mu, \kappa_{\mathrm{P}})$ [12] and for $\chi_{\mathrm{T}} = 0$. That is, the phenomenological derivation of the preceding section was based on a purely reciprocal effect. A Tellegen material is well beyond the scope of this text, but suffice it to say that it is a complex material having bound-electric and magnetic permanent dipoles. A Pasteur material is an isotropic chiral material, where the axial direction of the helices are uniformly randomly oriented. An alignment of the helical axes makes the material anisotropic, which has the implication that κ_{P} becomes a tensor.

In the following analysis, a lossless, reciprocal, bi-isotropic medium is considered. The constitutive relations (3.8.11) form the scalar transfer relation

$$\mathbf{C}_{EH} = \begin{pmatrix} \varepsilon & -j\kappa_{\mathrm{P}} \\ j\kappa_{\mathrm{P}} & \mu \end{pmatrix} \tag{3.8.12}$$

The kDB formalism requires the inverse constitutive relations $\mathbf{C}_{DB} = \mathbf{C}_{EH}^{-1}$. The bi-isotropic kDB constitutive relations are written as

$$\mathbf{E} = \kappa\mathbf{D} + j\chi\mathbf{B} \tag{3.8.13a}$$

$$\mathbf{H} = -j\chi\mathbf{D} + \nu\mathbf{B} \tag{3.8.13b}$$

There is no transformation of the constitutive parameters into kDB, as they are all scalars. Substitution into the coupled kDB equations (3.3.5) yields

$$\kappa \begin{pmatrix} D_1 \\ D_2 \end{pmatrix} = -\begin{pmatrix} j\chi & -u \\ u & j\chi \end{pmatrix} \begin{pmatrix} B_1 \\ B_2 \end{pmatrix} \tag{3.8.14a}$$

$$\nu \begin{pmatrix} B_1 \\ B_2 \end{pmatrix} = -\begin{pmatrix} -j\chi & u \\ -u & -j\chi \end{pmatrix} \begin{pmatrix} D_1 \\ D_2 \end{pmatrix} \tag{3.8.14b}$$

Elimination of $\mathbf{B}$ generates the governing equation

$$\begin{pmatrix} u^2 + \chi^2 - \kappa\nu & 2ju\chi \\ -2ju\chi & u^2 + \chi^2 - \kappa\nu \end{pmatrix} \begin{pmatrix} D_1 \\ D_2 \end{pmatrix} = 0 \tag{3.8.15}$$

The eigenvectors of (3.8.15) are circular states:

$$|r_+\rangle = \begin{pmatrix} 1 \\ j \end{pmatrix}, \quad |r_-\rangle = \begin{pmatrix} 1 \\ -j \end{pmatrix} \tag{3.8.16}$$

with corresponding phase-velocity eigenvalues

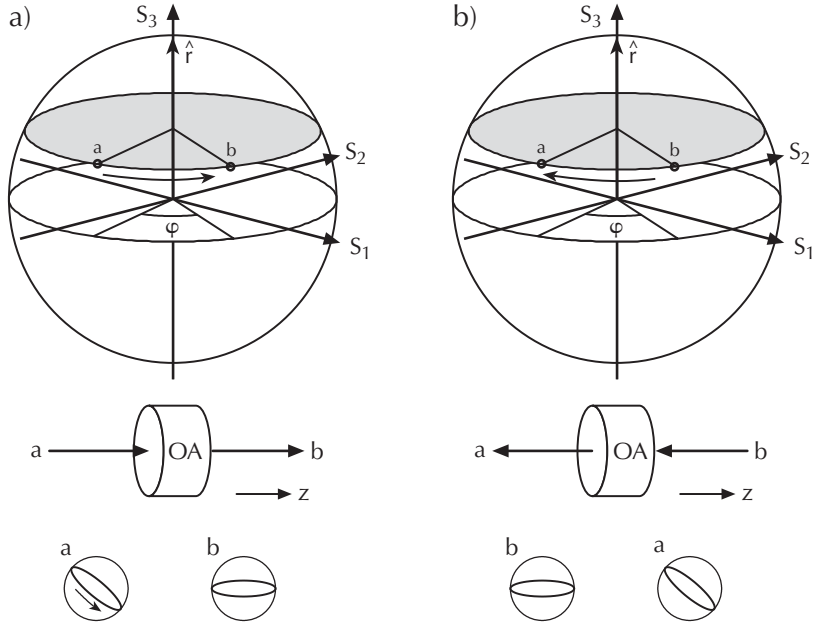

Fig. 3.22. An optically active medium is reciprocal. a) Forward travel. The precession axis is $+S_3$; the eigenvectors are circular polarization states. Transit through the medium transforms an input polarization state from (a) to (b). b) Backward travel. The precession axis remains $+S_3$. Transit through the medium transforms input polarization state (b) to (a).

$$u_{\pm} = \sqrt{\kappa\nu} \pm \chi \tag{3.8.17}$$

The corresponding wavenumbers are

$$k_{\pm} = \frac{\omega}{c} \frac{n}{1 \pm n\chi/c} \tag{3.8.18}$$

where n is an average index. For positive χ values, right-hand circularly polarized light travels slower than left-hand polarization.

As the constitutive relations in the present model are scalars, the Poynting vector coincides with the k-vector in the medium. Polarization transformation therefore occurs through transit. In Stokes space, the precession axis $\hat{r}$ points along $+S_3$. The precession angle is determined by the phase difference (3.7.28). The transformation matrix U is therefore

$$U = \begin{pmatrix} \cos(\varphi/2) & -\sin(\varphi/2) \\ \sin(\varphi/2) & \cos(\varphi/2) \end{pmatrix} \tag{3.8.19}$$

For positive χ values the precession in Stokes space for $+z$ travel follows $|\varphi|$.

Polarization transformation due to optical activity is similar to that of Faraday rotation: the precession axes for both mechanisms are $\pm S_3$. This is in stark contrast to birefringent transformation where the precession axis lies in the (S_1, S_2) plane. However, unlike Faraday rotation, when $\chi_T = 0$ optically active media is reciprocal (see Fig. 3.22). Consider the upper-right-hand matrix component from Faraday and OA governing equations (3.7.13, 3.8.15):

Faraday	$-j\kappa_g \nu \cos\theta$
Optical Activity	$2ju\chi$

For Faraday rotation, the sign of the off-diagonal term changes when the propagation direction is reversed. This is not the case with optical activity, where the sign is unaffected by direction. Therefore the eigenvectors for OA do not change when the propagation direction is reversed.

Like Faraday rotation, a chiral medium will rotate a linear polarization state from one angle to another. The rotary power ρ of a chiral material is this polarization rotation per unit length. From the above analysis, the rotary power is $\rho = \varphi/2z$. Biot's law (circa 1812) gives a phenomenological although rather accurate wavelength dependence of the rotary power:

$$\rho = a + \frac{b}{\lambda^2} \tag{3.8.20}$$

Drude in the nineteenth century proposed an extension of Biot's to account for multiple material resonances, akin to Sellmeier's equations. Drude's equation is

$$\rho = \sum_i \frac{b_i}{\lambda^2 - \lambda_o^2} \tag{3.8.21}$$

These models are complex to derive. For more information on the relevant expressions and the tools required for derivation, see [10].

References

1. H. Ammari, K. Hamdache, and J. Nédélec, "Chirality in the Maxwell equations by the dipole approximation," *SIAM Journal of Applied Math.*, vol. 59, pp. 2045–2059, 1999.
2. D. J. Caldwell and H. Eyring, *The Theory of Optical Activity.* New York: Wiley-Interscience, 1971.
3. M. N. Deeter, G. W. Day, and A. H. Rose, *CRC Handbook of Laser Science and Technology, Supplement 2: Optical Materials.* Boca Raton, Florida: CRC Press, 1995, ch. Magnetooptic Materials, pp. 367–402.
4. F. Fedorov, "On the theory of optical activity of crystals. I. Energy conservation law and optical activity tensors, optics and spectroscopy," *Optics and Spectroscopy*, vol. 6, pp. 85–93, 1959.
5. G. R. Fowles, *Introduction to Modern Optics.* New York: Dover Publications, 1989.
6. V. J. Fratello and R. Wolfe, *Handbook of Thin Film Devices, Vol. 4: Magnetic Thin Film Devices.* San Diego: Academic Press, 2001, ch. Epitaxial Garnet Films for Nonreciprocal Magneto-Optic Devices, pp. 93–141.
7. D. J. Hagan, private communication, 2002, from lecture notes, School of Optics, University of Central Florida. [Online]. Available: http://www.creol.ucf.edu/
8. H. A. Haus and J. R. Melcher, *Electromagnetic Fields and Energy.* Englewood Cliffs, New Jersey: Prentice–Hall, 1989.
9. A. Jain, J. Kumar, F. Zhou, L. Li, and S. Tripathy, "A simple experiment for determining verdet constants using alternating current magnetic fields," *Am. J. Phys.*, vol. 67, pp. 714–717, 1999.
10. W. Kaminsky, "Experimental and phenomenological aspects of circular birefringence and related properties in transparent crystals," *Rep. Prog. Phys.*, vol. 63, pp. 1575–1640, 2000.
11. J. A. Kong, *Electromagnetic Wave Theory.* New York: John Wiley & Sons, 1989.
12. I. Lindell, A. Sihvola, S. Tretyakov, and A. Viitanen, *Electromagnetic Waves in Chiral and Bi-Isotropic Media.* Boston, Massachusetts: Actech House, 1994.
13. K. B. Rochford, A. H. Rose, and G. Day, "Magneto-optic sensors based on iron garnets," *IEEE Transactions on Magnetics*, vol. 32, no. 5, pp. 4113–4117, 1996.
14. K. Shirai, K. Ishikura, and N. Takeda, "Low saturated magnetic field bismuth-substituted rare earth iron garnet single crystal and its use," U.S. Patent 5,512,193, Aug. 30, 1996.
15. K. Shirai and N. Takeda, "Faraday rotator," U.S. Patent 5,535,046, July 9, 1996.